Moisture Tolerance, Thermally Stable and Light Switchable Adhesives Platform Based on Reversible Redshifted [2+2] Photocycloaddition

Xin Yi Oh, Quyen Thi Vu, Michelle Yu Mei Ling, Mohammad Izadyar, Syed Ali Abbas Abedi, Xiaogang Liu, Vinh X. Truong**

Xin Yi Oh, Quyen Thi Vu, Michelle Yu Mei Ling, Vinh X. Truong
Institute of Sustainability for Chemicals, Energy and Environment (ISCE2), Agency for Science, Technology and Research (A*STAR), 1 Pesek Road, Jurong Island, Singapore, 627833, Republic of Singapore.
Mohammad Izadyar, Syed Ali Abbas Abedi, Xiaogang Liu
Fluorescence Research Group, Singapore University of Technology and Design, 8 Somapah Road, Singapore 487372, Republic of Singapore
E-mail: oh_xin_yi@isce2.a-star.edu.sg; vinh_truong@isce2.a-star.edu.sg

Keywords: adhesives, photocycloaddition, visible light, light switchable cycloreversion, pyrene, DFT calculations, moisture-tolerance.

Adhesives are essential in the manufacturing of modern technological devices for various application fields, ranging from transportation to communications, to aerospace and energy generation and storage. Their adhesion strength and stability are critical for the device's development and performance; however, they pose significant challenges to disassembly and recycling. These challenges can be overcome by introducing user-defined debondable or reversible technologies into structural adhesives. Herein, we report a new adhesive formulation that can be bonded and detached by blue light (λ = 410–450 nm) and UV light (λ = 340–355 nm), respectively. The adhesive platform is prepared by incorporating acrylamidyl pyrene moieties into polyethylenimine, enabling reversible photocrosslinking by redshifted [2+2] photocycloaddition. The photophysical properties and switching mechanisms between the monomeric and dimeric forms of the acrylamidyl pyrene were thoroughly investigated by spectroscopic measurements and complemented by comprehensive quantum chemical calculations. Under selective irradiation of low-energy blue and UV light, the reversible photocycloaddition [2+2] facilitates dynamic bonding and debonding of the crosslinked networks, enabling reversible adhesion between a range of solid substrates. Critically, the adhesives are stable at elevated temperatures above 70 °C and in aqueous environments,

thereby providing a new strategy for the development of next-generation debonding on-demand adhesives.

1. Introduction

Adhesion between substrates plays an important role in our daily lives, providing the means to connect and assemble various solid components. Such bonding functions are also essential for constructing complex materials in manufacturing industries. While conventional glues originated from epoxies, acrylates, and urethanes have been widely used to provide strong adhesion with robust bonding strength,[1-8] these adhesives are non-responsive and difficult to recycle. In addition, their adhesive performance deteriorates significantly when exposed to aqueous environments, as water can interact and inhibit the bonding processes or degrade the crosslinked polymer structures. Thus, modern adhesive technologies are transitioning towards new platforms that can provide robust bonding and rapid detachment on-demand, i.e., in response to an external stimulus such as electricity,[9-12] pH,[13-14] heat,[15-16] or light.[17-24] The concept of an easy-to-handle tacky resin that can enable switchable adhesive structure under an external stimulus is highly desirable for structural materials, as well as for advanced applications in semiconductors and biomedicine.[25-28] In addition, responsive and reversible adhesives feature the enticing prospect of repair and recyclability,[29-31] thereby contributing to a circular economy.

Among the stimuli introduced for on-demand activation/deactivation of the adhesive function, light is highly attractive due to its precise spatial and temporal control. Light operation techniques are non-intrusive and can also be of low cost when the materials are responsive to wavelength in the visible region. To date, photo-reversible adhesives have been developed based on chromophores that can undergo interconvertible structural changes, such as azobenzenes,[17, 21, 24, 32-34] diarylethenes,[35-37] and spiropyran[38-40]. Furthermore, several adhesive systems have been developed based on chromophores that can participate in reversible photocycloaddition systems, including [4+4] photodimerization of anthracenes[41-43] or [2+2] photodimerization of cinnamate[44] which further requires thermal activation for adhesion and coumarin[45-46] derivatives. Many of these systems employ UV light (λ = 300–400 nm) for activation and even shorter UV wavelength (λ = 240 nm) for deactivation. In general, the use of high energy and short wavelength UV light poses several limitations: (i) the materials must be in close contact with the light source since short wavelength UV light has low penetrating power; (ii) generation of high energy UV light can be energy demanding; and

(iii) high energy UV light can be damaging due to oxidative degradation, while also being harmful to human health.[47-48]

Herein, we introduce a reversible adhesive system in which the bonding and debonding can be initiated by visible light (λ= 400–500 nm) and UV light (340–350 nm), respectively (**Figure 1)**. Our system is based on an acrylamidyl pyrene (AP) chromophore that can undergo cycloaddition by blue light, forming a cyclobutane that can be cleaved back to the starting chromophore by long-wavelength UV light. We identify the mechanism and activation-free energies for the cycloaddition and dissociation by quantum chemical calculations, providing the basic parameters for experimental setup in the bonding/debonding of the adhesives. The adhesives can be readily prepared by attaching the chromophores to a commercial polyethylene imine (PEI), forming an easy-to-handle **AP-PEI** resin in high yield. We further demonstrate the reversible adhesive properties of the **AP-PEI** for on-demand bonding/debonding of solid substrates in aqueous environments.

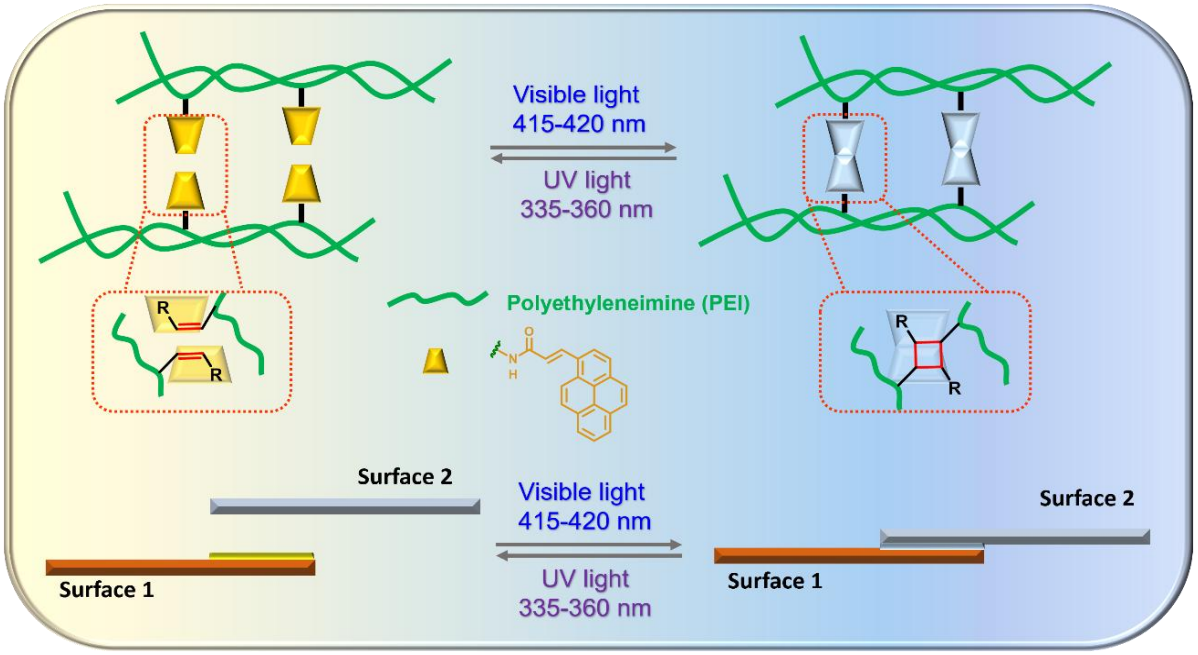

Figure 1. Design of wavelength-selective bond- and debondable adhesive platform based on redshifted photocycloaddition. The adhesive formulation consists of polyethylene imine (PEI) functionalized with acrylamidyl pyrene (**AP**) chromophore that can undergo redshifted [2+2] photocycloaddition, enabling photocrosslinking and degradation by blue light and UV light, respectively. The photo-reversible crosslinked structure provides cohesion, while interfacial adhesion is endowed by the hygroscopic and hydrophilic **AP-PEI** glue.

2. Results and Discussion

2.1 Light-activated cycloaddition and cycloreversion of small molecule pyrene amide

To establish the irradiation conditions and the underlying mechanism for the reversible photocycloaddition of the acrydylpyrene moiety, we first synthesized a small molecule, **AP** (**Figure 2,** compound **1**). This molecule can be readily prepared from pyrenecarboxaldehyde and propylamine as described in the supplementary information (SI). The synthesis is facile and can be upscaled to multigram. Such a protocol can also be readily applied to the large-scale synthesis of the modified polymer. Chromophore **1** undergoes photocycloaddition to form **1a** and **1b** under blue light irradiation, and photocycloreversion occurs under UV light irradiation (**Figure 2a**). The **AP** monomer is soluble in ethanol and ethyl acetate, whereas the **AP** dimer is not soluble in these solvents. As a result, we selected DMSO as the solvent for UV-Vis spectroscopy. UV-Vis spectrum of **1** in DMSO shows maximum absorbance at 370 nm, and the absorbance extends to 400 nm, while the cyclobutane adduct (**1a** and **1b**) displays absorbance at 330–350 nm (**Figure 2b**), extending into the blue light region (400–450 nm). The blue light activation is significantly redshifted compared to conventional cinnamic acid which can only be activated by UV light.[49] It should be noted that pyrene-based [2 + 2] chromophores have been reported to display redshifts in photoreactivity compared to their absorption spectra.[50-53] Thus, it may be possible to induce the photocycloaddition with light of longer wavelengths. Therefore, we select an LED light source with the irradiance centered at λ_{max} = 420 nm (intensity I = 20 mW·cm^{-2}) to initiate the photocycloaddition and a UV light source with the irradiance centered at λ_{max} = 355 nm (I = 4.78 mW·cm^{-2}) to study the photocycloreverison (**Figure S1**). The key advantage of our system is its use of longer wavelength activation for both bonding and debonding processes, in contrast to the UV light activation typically used for cinnamic acid derivatives.

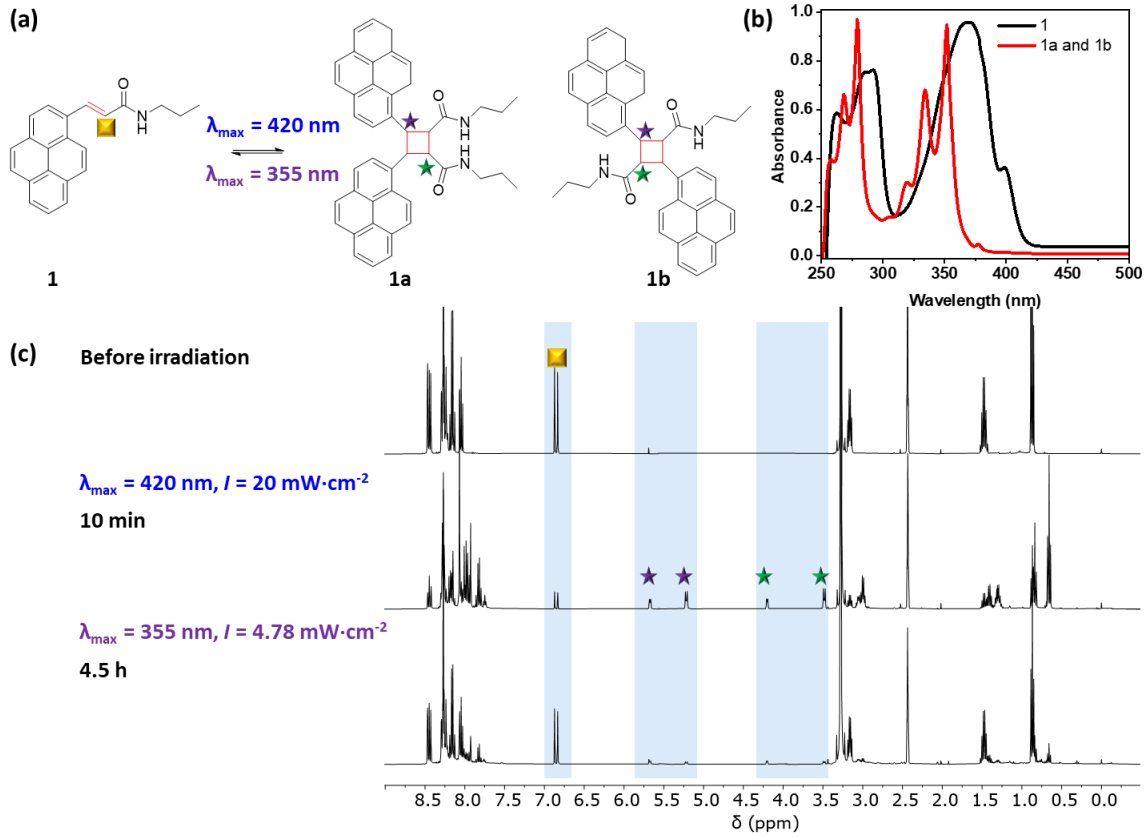

Figure 2. (a) Scheme of the reversible photodimerization of the model compounds (**1** and **1a**/**1b**) by blue and UV lights, respectively. **(b)** UV-Vis spectra of the model compounds in DMSO before (black line, **1**) and after (red line, **1a**/**1b**) blue light irradiation. **(c)** ^{1}H NMR spectra of **1** (400 MHz, DMSO-d_6) after blue light irradiation, followed by UV light irradiation.

The light-induced cycloaddition and cycloreversion processes were further confirmed by ^{1}H NMR spectroscopy. Under blue light irradiation, the chemical resonances of the alkene proton of **1** at 6.8 ppm rapidly decrease, followed by the concomitant increase of the resonances corresponding to the cyclobutane adduct (**1a** and **1b)** in the 5–5.8 ppm and 3.4–4.3 ppm regions (**Figure 2c**) with a conversion of 47% in 10 minutes. When the dimer adduct was irradiated with UV light λ_1 (λ_{max} = 355 nm; I = 4.78 mW·cm^{-2}), photocycloreversion was confirmed by the decrease of chemical resonances corresponding to the butane moiety (**Figure 2c**) with a final conversion up to 83%. Further irradiation at the dimer with 340 nm wavelength did not increase the conversion and thus complete cycloreversion could not be achieved. This is likely because the monomer **AP** also absorbs like in the 340–360 nm region, and photocycloaddition can therefore occur concurrently with cycloreversion. Therefore, an equilibrium of the monomer and dimer at the ratio of 17/83 was formed by UV light irradiation. Nevertheless,

this degree of reversion is suitable for photo-degradation of polymer network, as shown in our subsequent investigation.

In our NMR studies, we select a low-intensity UV light source to minimize the sample's thermal build-up and heating, thus affecting the cycloreversion. Indeed, under such an intensity, the temperature of the solution remained below 30 °C. Whereas some heating was observed when intensity was increased to 20 $mW \cdot cm^{-2}$, and monitoring of the sample showed an increase to 40 °C. Nevertheless, heating the mixture of **1a** and **1b** at a temperature of 80 °C for 4 h did not induce any cycloreversion reaction as indicated by the NMR spectrum.

To further understand if the photocycloreversion occurs more efficiently under irradiation of shorter wavelengths, we studied the reaction in λ_{max} = 345 nm (λ_2, intensity I = 4.14 $mW \cdot cm^{-2}$) and λ_{max} = 338 nm (λ_3, intensity I = 4.46 $mW \cdot cm^{-2}$). A low-intensity UV light was selected to prevent the heating of the NMR sample. The photocycloreversion rate after 0.5 h's irradiation for λ_1, λ_2, λ_3 were 29%, 34%, and 39%, respectively (**Figure S4b**). Photocycloreversion increased over time without any side reactions, from 29% to 83% (λ_1)., 34% to 83% (λ_2), and 39% to 84% (λ_3). The results thus suggested that all three wavelengths showed significant photocycloreversion up to 83% and above with a similar rate. Therefore, we chose λ_1 (λ_{max} = 355 nm) for further photoswitchable adhesive study. The kinetics of light-induced cycloaddition and reversion is highly dependant on the light intensity (**Figure S4**), and faster conversion was observed by increasing the irradiation intensity.

Quantum chemical calculation of photocycloaddition and cycloreversion

Through comprehensive quantum chemical calculations, we have elucidated the photophysical properties and switching mechanisms between the monomeric and dimeric forms of **1**. Our findings indicate that the dimeric form of **1** exhibits greater stability than its monomeric counterpart in DMSO, with a Gibbs free energy difference of 0.28 eV (**Figure 3a**). This enhanced dimer stability arises from forming two additional single bonds in the dimer. Furthermore, transitioning between the monomeric and dimeric forms entails overcoming a substantial energy barrier of 2.67 eV associated with the simultaneous cleavage of these two bonds in the ground state (**Figure S2**). Based on these insights, it is expected that UV light at 330–350 nm can be an effective energy wavelength to facilitate the disassociation of these bonds, thereby aiding the transition from the dimeric back to the monomeric form.

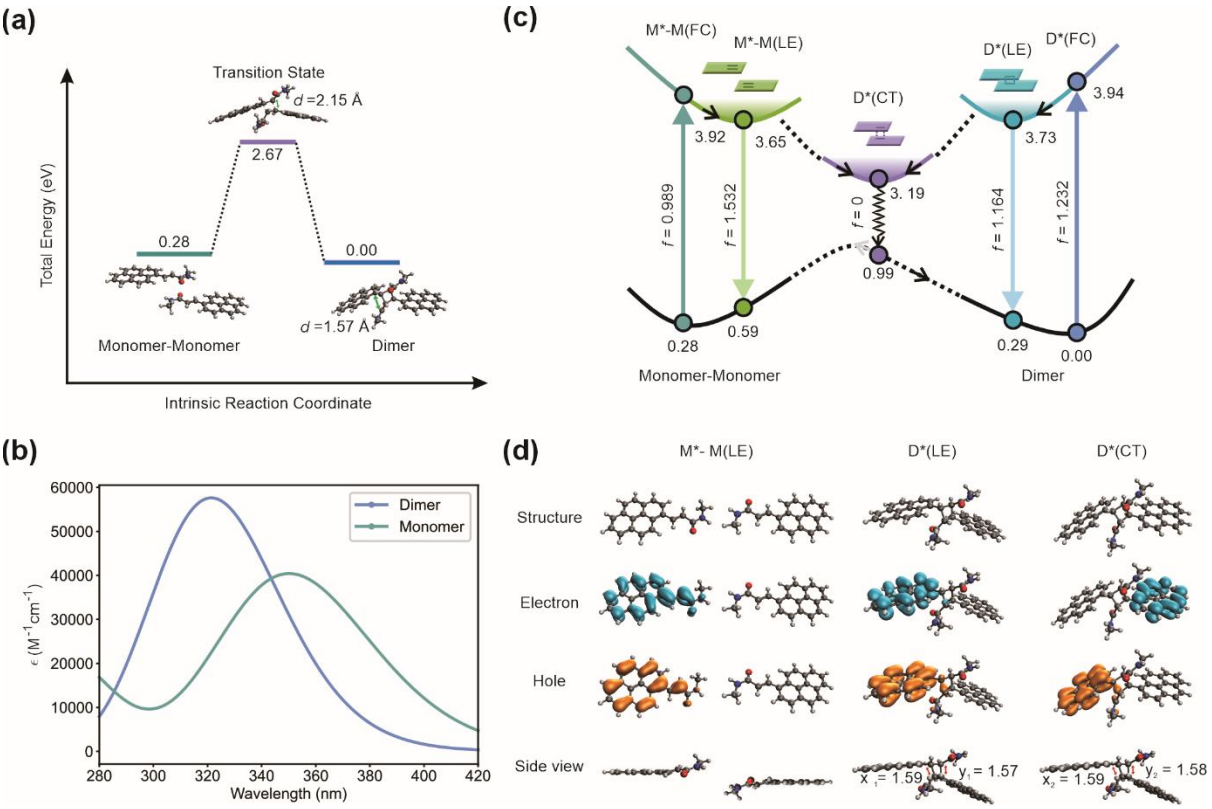

Figure 3. **(a)** Relative energy along the intrinsic reaction coordinate, comparing monomeric and dimeric states of **1**. The monomer-monomer state is less stable by 0.28 eV than the dimer, with an energy barrier of 2.67 eV at the transition state. The critical bond distances are annotated for each state. **(b)** Calculated UV-Vis absorption spectra showing molar absorptivity (ε) of monomeric and dimeric forms, with the monomer exhibiting a redshift than the dimer. **(c)** Schematic illustration of the photoswitching cycles between the monomeric and dimeric forms. Abbreviations: FC, the Franck-Condon state; LE, locally excited states; CT, the charge transfer states. The inset highlights the energy values and oscillator strength (*f*). The drawing is not in scale for clarity. **(d)** Molecular structures in various states alongside visualizations of electron and hole distributions are shown in two views, highlighting the changes in electron density (blue) and hole density (orange), correlating with the transitions depicted in (c).

Our calculations further reveal that monomeric **1** displays longer UV-Vis absorption and emission wavelengths due to its extended π-conjugation, which also results in notably bright emission (**Figure 3b**). In contrast, dimeric **1b** exhibits shorter, blue-shifted wavelengths and significantly lower quantum yield. Electron transfer occurs between the two pyrene derivatives in the dimer upon photoexcitation, leading to a low-lying charge transfer (CT) state (**Figure S3**). This CT state is non-emissive, characterized by an oscillator strength of zero. It is more stable than the emissive, locally excited state of each pyrene derivative. As a result, the dimeric

form of **1b** displays much dimmer luminescence compared to the monomeric form. The formation and stability of this CT state are pivotal in mediating the photoswitching between the monomeric and dimeric forms.

We conducted detailed excited state calculations to gain insights into the photoswitching mechanism of **1b** from its monomeric to dimeric form (**Figure 3c, d**). These calculations highlighted three pivotal species involved in this process. Initially, monomeric **1** absorbs light, transitioning to its locally excited S_1 state: M*-M(LE). This excited molecule (M*) has two pathways from this state: it can return to the ground state via fluorescence or non-radiative decay; alternatively, it can engage with the nearby monomeric unit in the ground state to form a molecular complex. Within this complex, electron transfer occurs between the two monomeric units. The resultant robust electrostatic interactions between the oppositely charged species drive the formation of a stable charge transfer (CT) state, which is critical for the transition to the dimeric form (**Figure 2c, d**).

This charge transfer (CT) state of the dimeric **1b** features two single bonds between the pyrene derivatives. Due to its biradical nature, this charge transfer state is non-emissive and exhibits high reactivity. Following charge recombination within these species, it reverts to the ground state and forms the dimeric **1b**, effectively completing the photoswitching process from monomeric to dimeric forms (**Figure 2d**). Upon photo-exciting the dimer, the pyrene derivative can also be switched from the dimeric to the monomeric form via the charge-transfer (CT) state. However, this dimer-to-monomer switching is less efficient than monomer-to-dimer switching because it involves the dissociation of the biradical. This calculation outcome agrees with our experimental data that a higher energy wavelength is required for cycloreversion.

2.2 AP-PEI with photoswitchable adhesive function

There is a growing demand for controlling the adhesiveness of materials to facilitate bonding and debonding on demand through various triggers. Such responsive capabilities not only allow for the development of smart materials, but also contribute significantly to environmental sustainability efforts. Having confirmed the responsiveness of our AP chromophore to visible and UV light, we subsequently designed an AP polymer with a light switchable adhesive function. We chose PEI as the polymer matrix due to its commercial availability and stability against oxidation post-modification.[54-55] In a typical protocol, **AP_1-PEI** was prepared by reacting an activated *N*-hydroxy succinimide ester with PEI. The degree of substitution can be calculated using a calibration curve from the UV-Vis absorbance of the small molecule **AP (Figure S5)**. We also prepared **AP-PEI** with increased amounts of **AP**,

having molar ratios of 2 to 1 and 3 to 1, respectively (**Table S1**), namely **AP$_2$-PEI** and **AP$_3$-PEI**. Subsequently, we use these **AP-PEI** as responsive adhesives under visible and UV light.

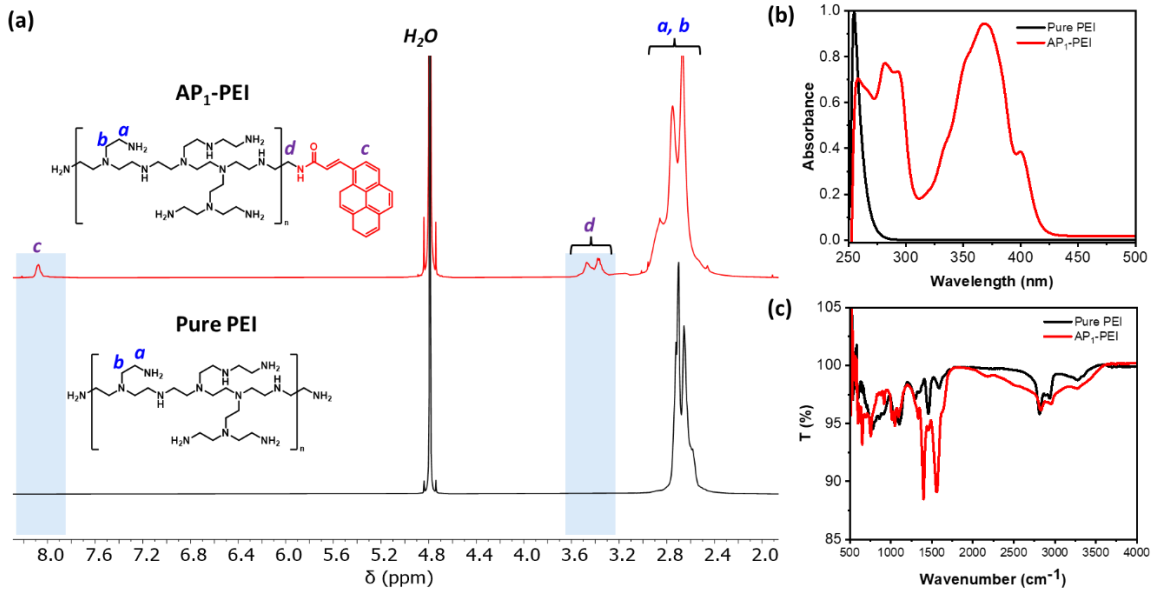

Figure 4. Characterization of **AP-PEI**. **(a)** ^{1}H NMR spectrum of **AP$_1$-PEI** (top) together with the spectrum of pure PEI (bottom) showing the incorporation of **AP** (400 MHz, D_2O). **(b)** UV-Vis spectrum of **AP$_1$-PEI** (red line) together with the spectrum of pure PEI (black line), showing the maximum absorbance of **AP** at 370 nm to 400 nm in water. **(c)** FTIR spectrum of **AP$_1$-PEI** (red line) and the spectrum of pure PEI (black line), showing the C=O stretching of the amide moiety at 1560 cm^{-1} and 1400 cm^{-1}.

^{1}H NMR spectroscopy of **AP$_1$-PEI** in water shows chemical resonance at 8.1 ppm (blue region), corresponding to the pyrene protons of **AP** chromophore, and 3.4–3.5 ppm (blue region) corresponding to the methylene proton neighboring to the amide moiety, which are not seen in pure PEI (**Figure 4a**). The UV-Vis spectrum also confirmed the presence of **AP** chromophore in **AP$_1$-PEI** in water with maximum absorbance at 370 nm, and the absorbance extends to 400 nm (**Figure 4b**). FTIR spectrum of **AP$_1$-PEI** shows C=O stretching of the amide moiety at 1560 cm^{-1} and 1400 cm^{-1}, which are absent from pure PEI, indicating the incorporation of **AP** chromophore to PEI via the formation of amide linkage (**Figure 4c**). Furthermore, **AP$_1$-PEI** also displays fluorescence properties similar to compound **1**, whereas PEI is non-fluorescent (**Figure S5**). Collectively, all these results indicate the successful incorporation of the **AP** function into PEI. To estimate the degree of substitution of **AP** in **AP$_1$-PEI**, we set up a standard curve by measuring the absorbances of compound **1** in a range of

known concentrations (**Figure S6**). Using this standard curve, concentration of **AP** was calculated to be 5.66 µM in a 1 mg/mL **AP$_1$-PEI** solution.

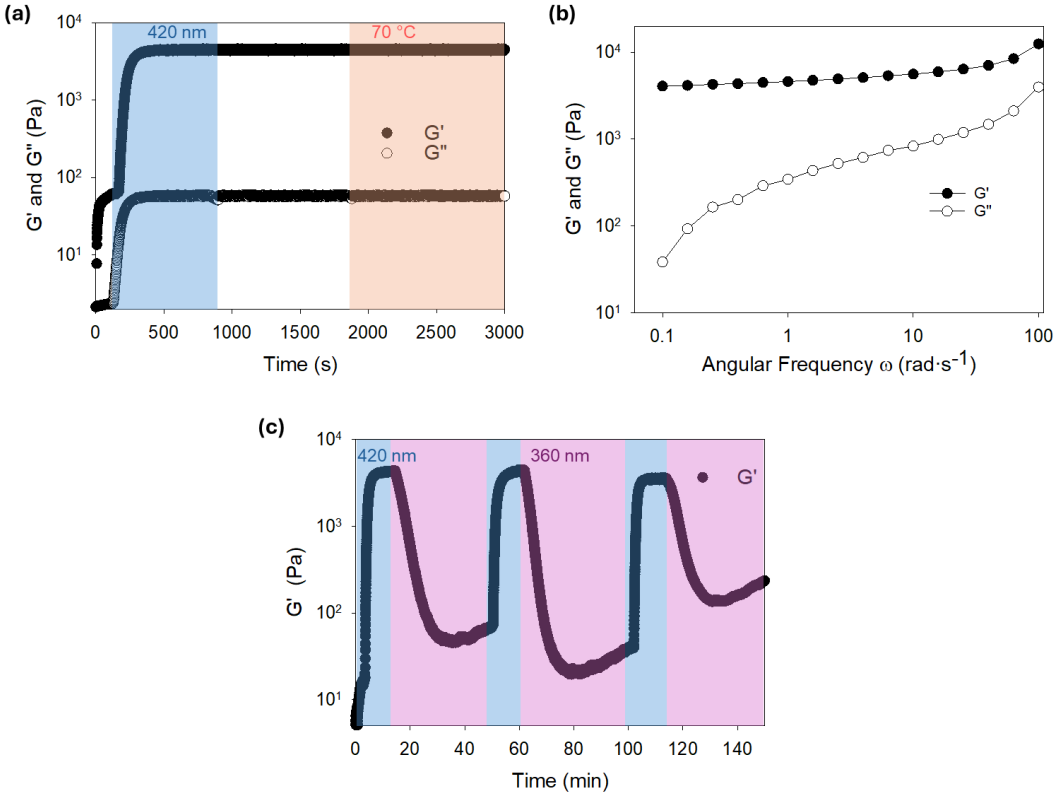

Figure 5. (a) Rheological assessment (time sweep) of **AP$_1$-PEI** (50 wt% in water**)** under irradiation of blue light (λ_{max} = 420 nm, I = 20 mW·cm^{-2}), showing the rapid increase of G' value, the material was further heated at 70 °C post-photocuring which shows no change in the G' value; **(b)** Frequency sweep of the photocured **AP$_1$-PEI** showing the evolution of G' and G" values, indicating high cohesion and adhesion strength, respectively; **(c)** photo-cross-linking/de-cross-linking of **AP$_1$-PEI** under irradiations of alternating blue light (λ_{max} = 420 nm) and UV light (λ_{max} = 340 nm) at the intensity I = 10 mW·cm^{-2} using an Omnicure lamp.

Subsequently, the photo-crosslinking of **AP-PEI** resins was investigated by rheology measurements. We prepared **AP$_1$-PEI** (50 wt% in water), **AP$_2$-PEI** (30 wt% in water), and **AP$_3$-PEI** (30 wt% in water). The further dilution of **AP$_2$-PEI** and **AP$_3$-PEI** was due to their poor solubility in water, resulting from a higher degree of substitution of the AP moiety. The storage modulus (G') value of **AP$_1$-PEI** increased significantly from *ca.* 10 Pa to 5.1 kPa (**Figure 5a**) under blue light (λ_{max} = 420 nm) irradiation, indicating the formation of a robust network structure and cohesion strength. Based on our small molecule study, [2+2]

photocycloaddition reached near completion under the employed irradiation conditions. Thus, the rapid increase in storage modulus is from photo-induced crosslinking. The photocrosslinking reaction occurred almost immediately after irradiation with blue light (λ_{max} = 420 nm, 0.1 W), and plateau was achieved in less than 5 min under this mild irradiation condition. In addition, the G" value was lower than G' both before and after photocrosslinking, indicating the gel-like and tacky nature of the adhesive material.

To assess the stability of the crosslinked material, the temperature was increased to 70 ^{o}C. Under this temperature, the photo-crosslinked **AP$_1$-PEI** displayed no change in G' value, indicating its thermal stability (**Figure 5a**). For **AP$_2$-PEI** and **AP$_3$-PEI** (30 wt% in water), their G' values also displayed a rapid increase under blue light irradiation similar to **AP$_1$-PEI**, but not to a higher extent even with a higher proportion of AP units (**Figure S7**). This could be due to the less soluble **AP$_2$-PEI** and **AP$_3$-PEI** in water due to the higher percentage of hydrophobic pyrene units, forming a heterogeneous mixture and reducing photo-crosslinking efficiency. Furthermore, while crosslinking is critical for the cohesion, excessive crosslinking will reduce the adhesion strength due to that the crosslinking hinders the mobility of molecular chains and makes the film rigid.[56-57]

Frequency sweep on the cured polymer showed an increase in both G' and G" values, which are characteristics of high cohesive and adhesive strength, respectively (**Figure 5b**). Furthermore, adding water to the photo-crosslinked **AP$_1$-PEI** and submerging it in water for 8 h resulted in only a slight decrease in the G' value to 4.8 kPa, indicating the structural stability in the aqueous environment post-photocuring. The crosslinked structure was rapidly decoupled under UV light (λ_{max} = 340 nm, I = 10 mW·cm^{-2}) irradiation, reaching the modulus of ca. 40 Pa within 10 min (**Figure 5c**). The degraded network can be re-crosslinked by switching the irradiation wavelength from UV to blue light, forming the bonded network without any loss in the storage modulus. We have thus demonstrated three cycles of wavelength-selective bonding and debonding under blue light and UV light, respectively. It was observed that prolonged exposure to UV light post-debonding resulted in a slow increase in the storage modulus, possibly due to the evaporation/drying of water in the resin formulation.

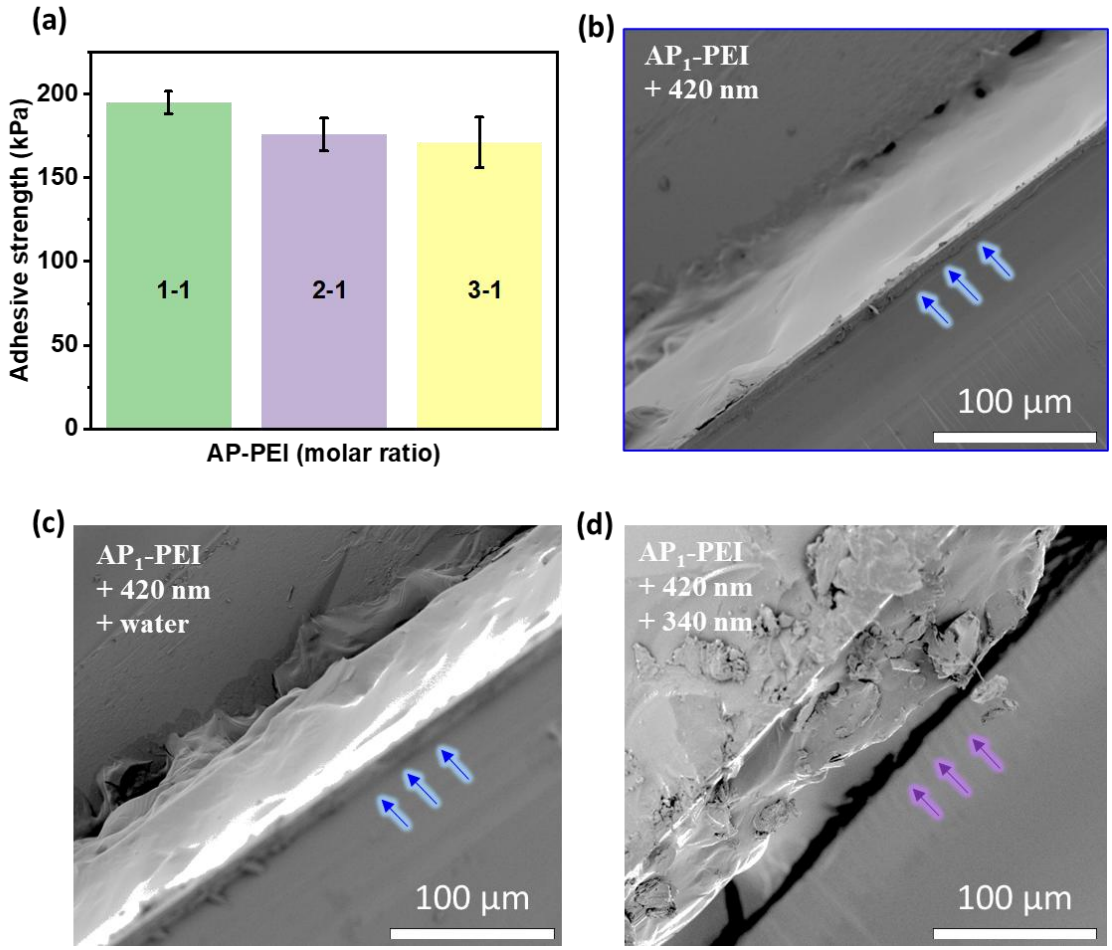

Figure 6. **(a)** Adhesive strength of **AP-PEI** resins with different degrees of AP substitution after blue light (λ_{max} = 420 nm, I = 20 mW cm^{-2}, 10 min) curing on glass substrates; SEM images of the cross-section between the glass substrates of **(b) AP$_1$-PEI** post-curing (the blue arrows indicate the front-facing light irradiation), **(c) AP$_1$-PEI** adhesive after soaking in water for 2 h, and **(d) AP$_1$-PEI** adhesive after irradiation with UV light for (λ_{max} = 340 nm, I = 10 mW cm^{-2}, 10 min).

The adhesive strength of photo-crosslinked **AP-PEI** was subsequently evaluated using a tensile tester. To prepare the sample, we applied **AP-PEI** resin directly onto the glass substrate and placed another substrate on top, followed by hand-pressing the substrate for 10 s. The resin-covered area was then exposed to blue light (λ_{max} = 420 nm, I = 20 mW·cm^{-2}) for 10 minutes, forming a strong adhesion between the two glass substrates. All three **AP-PEI** adhesive formulations show good adhesive strengths with values of 150-200 kPa. These adhesive strengths are comparable to the photo-adhesives prepared by UV-light-induced photocycloaddition of anthracene[43] or coumarin[45]. Similar to the rheology data, the substrates

can be readily debonded by UV light irradiation (λ_{max} = 340 nm, I = 10 mW·cm^{-2}) with the adhesion strength dropping below 1 kPa after 10 minutes of irradiation. The decrease in adhesion strength is believed to result from a reduction in crosslinking density (decrease in cohesion) caused by photocycloreversion. SEM images of the **AP$_1$-PEI** adhesive cross-section show a thickness of ca. 60 μm (**Figure 6b**), and no significant change in the adhesive thickness was observed after immersing the bonded substrate in water for 2 days, indicating no swelling occurring (**Figure 6c**). This may be due to the highly hydrophobic nature of the AP dimer, resulting from the π-π stacking and aggregation of the conjugated aromatic structures. SEM images of the UV light-exposed adhesive further reveal the fracture and detachment of the adhesive layer from the substrate front that was directly exposed to UV light (**Figure 6d**). This observation is interesting, as it indicates that the debonding mechanism occurs via both the loss of cohesion and adhesion under UV light irradiation. It was also observed that the residues remain at the adhesion interface after debonding with some interface showing adhesive detachment from the substrate (**Figure S8**). Based on the rheology data, it is possible to photo-cure the debonded residues to form adhesion again.

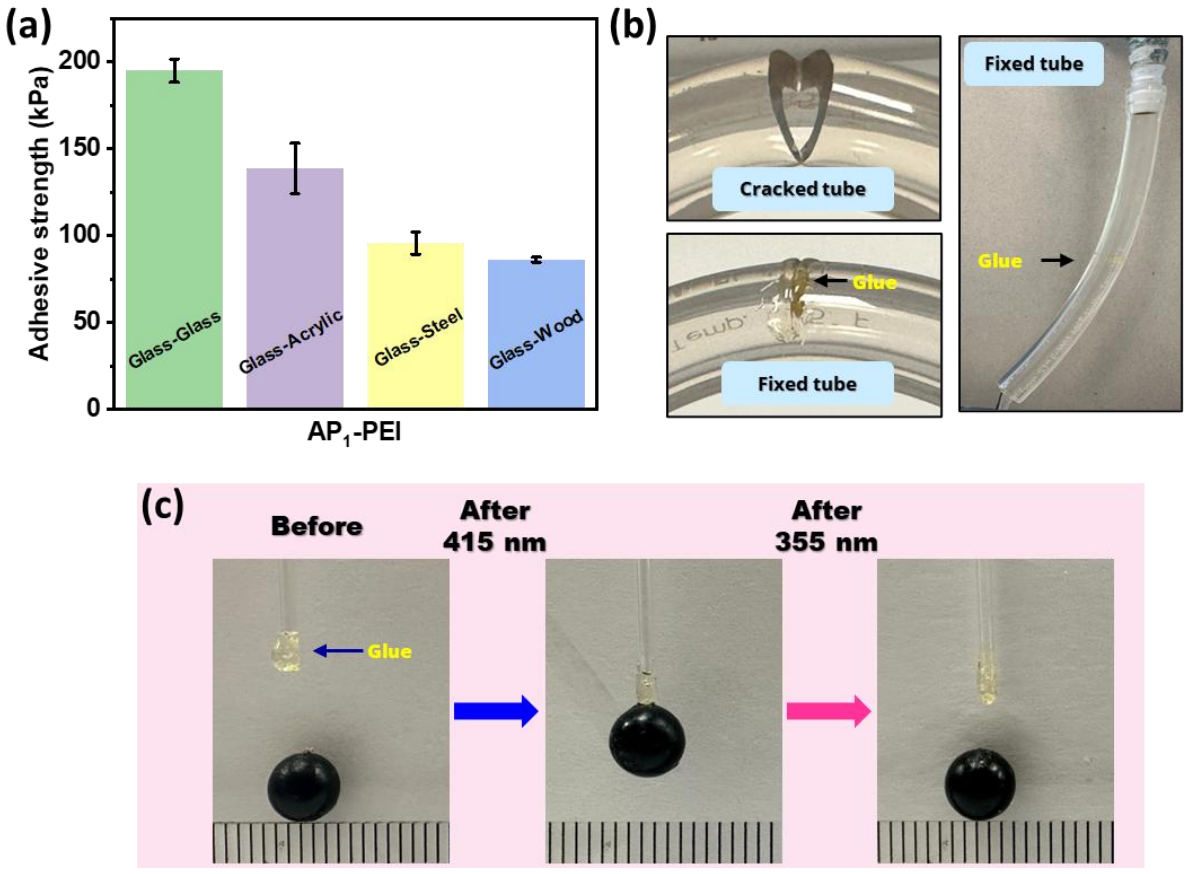

Figure 7. **(a)** Adhesive strengths of **AP$_1$-PEI** in different substrates after irradiation with blue light (λ_{max} = 420 nm, I = 20 mW·cm^{-2}); **(b)** Demonstration of **AP$_1$-PEI** as glue to fix cracked tube without any water leakage after irradiation with blue light; **(c)** Demonstration of **AP$_1$-PEI** as glue to carry a ball in a controllable manner. **AP$_1$-PEI** was in contact with the ball and glued it after blue light irradiation for 5 min (left and middle images). After UV light (λ_{max} = 355 nm, intensity I = 4.78 mW·cm^{-2}) irradiation for 10 min, the ball was released (right image).

To demonstrate the versatility of our adhesive performance across various substrates, we fixed one of the substrates to be glass and tested the photo-adhesion of **AP$_1$-PEI** on a range of substrates, including acrylic, wood, and stainless steel. The **AP$_1$-PEI** adhesive exhibited an impressive adhesive strength of nearly 200 kPa on a glass-glass substrate (**Figure 7a**). **AP$_2$-PEI** and **AP$_3$-PEI** showed similar but slightly lower adhesive strength at 176 kPa and 171 kPa, respectively. Furthermore, **AP$_1$-PEI** adhesive successfully bonded glass-acrylic (139±22 kPa), glass-steel (96±14 kPa), and glass-wood (86±4 kPa). The light switching adhesion was also realized on all these substrates, with efficient debonding under irradiation of long wavelength UV light (λ_{max} = 340 nm, I = 10 mW·cm^{-2}) within 10 minutes. Overall, the adhesive strength ranges from 86 to 200 kPa across various substrates, offering significant bonding strength. This level of adhesive strength is well-suited for peeling adhesive applications, which typically require a minimum of 80 kPa.[58]

We also demonstrated the use of **AP$_1$-PEI** adhesive in fixing a damaged substrate with an uneven surface, such as a fractured plastic tube. The **AP$_1$-PEI** can be readily applied on the cracked area and form strong adhesion upon blue light exposure, enabling the normal use of the damaged tube, such as running tape water without any leakage (**Figure 7b**). The remote control over the adhesion of **AP$_1$-PEI** resin was further highlighted in a demonstration of the capture and release of an object using simple handheld LED lights (**Figure 7c**). In this demonstration, we applied the **AP$_1$-PEI** resin on a glass capillary and contacted a black ball. It can be seen that our adhesive possesses sufficient viscosity (G' value of ca. 10 Pa, refer to **Figure 5a**) for handling as a resin before photocuring. Subsequently, adhesion was induced by blue light (λ_{max} = 420 nm, I = 20 mW·cm^{-2}) irradiation on the resin for 5 minutes, enabling the attachment of the ball, which can be lifted and moved. In the next step, we irradiated the adhered part with UV light (λ_{max} = 355 nm, intensity I = 4.78 mW·cm^{-2}) for 10 minutes, inducing the debonding and release of the ball.

3. Conclusion

In conclusion, we have demonstrated a photo-switchable adhesive platform based on PEI modified with a redshifted [2+2] AP chromophore, displaying adhesion strength from 86 kPa to 200 kPa across various substrates, including glass, acrylic, steel, and wood. The dimerization occurs under blue light (420 nm) with high efficiency, whereas the dimer adduct undergoes photocycloreversion upon exposure to 340–360 nm light, with a significant conversion of up to 83%. The photocrosslinking reaction, via dimerization, occurs rapidly, achieving high degree of crosslinking in under 5 minutes under mild irradiation conditions (blue LED light). Critically, the photo-crosslinked **AP$_1$-PEI** shows thermal stability up to 70 °C, whilst being readily degraded by UV light at 340–360 nm wavelength. The utilization of longer wavelength of UV light enables the use of versatile light sources, such as LED light for the debonding process. The photoreversible dimerization of the AP chromophore enables the formation of a dynamic polymer network, providing potential applications for responsive adhesives in aqueous environments and at elevated temperatures.

Acknowledgement

V.X.T. acknowledge funding support from the Industry Alignment Fund—Pre-Positioning Programme (IAF-PP: H23J2a0130) for the development of new polymer crosslinking technologies. V.X.T. and X.Y.O. are grateful for funding support from A*STAR in the form of Career Development Fund (23-8313GU). The research was also supported by the Singapore University of Technology and Design (SUTD) Kickstarter Initiative (SKI 2021_04_09). The authors are grateful for the computing service of SUTD and the National Supercomputing Centre (Singapore).

References

[1] H. Park, D. Lim, G. Lee, M.-J. Baek, D. W. Lee, *Advanced Functional Materials* **2023**, 33, 2305750.

[2] M. A. Droesbeke, R. Aksakal, A. Simula, J. M. Asua, F. E. Du Prez, *Progress in Polymer Science* **2021**, 117, 101396.

[3] A. M. Borrero-López, D. B. Guzmán, J. A. González-Delgado, J. F. Arteaga, C. Valencia, U. Pischel, J. M. Franco, *ACS Sustainable Chemistry & Engineering* **2021**, 9, 11032.

[4] F. Ascione, L. Granata, L. Guadagno, C. Naddeo, *Composite Structures* **2021**, 265, 113591.

[5] A. H. C. Anthis, X. Hu, M. T. Matter, A. L. Neuer, K. Wei, A. A. Schlegel, F. H. L. Starsich, I. K. Herrmann, *Advanced Functional Materials* **2021**, 31, 2007099.

[6] H. Wei, J. Xia, W. Zhou, L. Zhou, G. Hussain, Q. Li, K. Ostrikov, *Composites Part B: Engineering* **2020**, 193, 108035.

[7] L. A. Modesti, A. S. d. Vargas, E. L. Schneider, *International Journal of Adhesion and Adhesives* **2020**, 101, 102645.
[8] J.-H. Back, Y. Kwon, J. C. Roldao, Y. Yu, H.-J. Kim, J. Gierschner, W. Lee, M. S. Kwon, *Green Chemistry* **2020**, 22, 8289.
[9] J. Huang, Y. Liu, Y. Yang, Z. Zhou, J. Mao, T. Wu, J. Liu, Q. Cai, C. Peng, Y. Xu, B. Zeng, W. Luo, G. Chen, C. Yuan, L. Dai, *Science Robotics* **2021**, 6, eabe1858.
[10] S. Li, H. Tian, J. Shao, H. Liu, D. Wang, W. Zhang, *ACS Applied Materials & Interfaces* **2020**, 12, 39745.
[11] H. J. Kim, L. Paquin, C. W. Barney, S. So, B. Chen, Z. Suo, A. J. Crosby, R. C. Hayward, *Advanced Materials* **2020**, 32, 2000600.
[12] M. S. Akram Bhuiyan, J. D. Roland, B. Liu, M. Reaume, Z. Zhang, J. D. Kelley, B. P. Lee, *Journal of the American Chemical Society* **2020**, 142, 4631.
[13] C. C. Buron, T. Vrlinic, T. Le Gallou, S. Lakard, A. Bolopion, P. Rougeot, B. Lakard, *ACS Applied Polymer Materials* **2020**, 2, 5646.
[14] B. Jin, G. Zhang, J. Lian, Q. Zhang, X. Zhan, F. Chen, *Journal of Materials Chemistry A* **2019**, 7, 12266.
[15] Z.-Y. Guo, C.-X. Li, M. Gao, X. Han, Y.-J. Zhang, W.-J. Zhang, W.-W. Li, *Angewandte Chemie International Edition* **2021**, 60, 2.
[16] X. Li, Y. Deng, J. Lai, G. Zhao, S. Dong, *Journal of the American Chemical Society* **2020**, 142, 5371.
[17] T.-H. Lee, J.-H. Back, J.-S. Lim, G.-Y. Han, M.-B. Yi, Y. Kim, J.-H. Lee, S. Kim, H.-J. Kim, *Composites Part B: Engineering* **2024**, 272, 111175.
[18] D. Kim, H. Kim, W. Jeon, H.-J. Kim, J. Choi, Y. Kim, M. S. Kwon, *Advanced Materials* **2024**, 36, 2309891.
[19] T.-H. Lee, G.-Y. Han, M.-B. Yi, H.-J. Kim, J.-H. Lee, S. Kim, *ACS Applied Materials & Interfaces* **2021**, 13, 43364.
[20] W. Feng, L. Chu, M. B. de Rooij, D. Liu, D. J. Broer, *Advanced Science* **2021**, 8, 2004051.
[21] Z. Wu, C. Ji, X. Zhao, Y. Han, K. Müllen, K. Pan, M. Yin, *Journal of the American Chemical Society* **2019**, 141, 7385.
[22] D. Tan, X. Wang, Q. Liu, K. Shi, B. Yang, S. Liu, Z.-S. Wu, L. Xue, *Small* **2019**, 15, 1904248.
[23] Y. Ma, S. Ma, Y. Wu, X. Pei, S. N. Gorb, Z. Wang, W. Liu, F. Zhou, *Advanced Materials* **2018**, 30, 1801595.
[24] H. Akiyama, M. Yoshida, *Advanced Materials* **2012**, 24, 2353.
[25] N. Li, Y. Li, Z. Cheng, Y. Liu, Y. Dai, S. Kang, S. Li, N. Shan, S. Wai, A. Ziaja, Y. Wang, J. Strzalka, W. Liu, C. Zhang, X. Gu, J. A. Hubbell, B. Tian, S. Wang, *Science* **2023**, 381, 686.
[26] Y. Jiang, X. Zhang, W. Zhang, M. Wang, L. Yan, K. Wang, L. Han, X. Lu, *ACS Nano* **2022**, 16, 8662.
[27] B. R. Freedman, O. Uzun, N. M. M. Luna, A. Rock, C. Clifford, E. Stoler, G. Östlund-Sholars, C. Johnson, D. J. Mooney, *Advanced Materials* **2021**, 33, 2008553.
[28] Z. Pan, C. Guo, X. Wang, J. Liu, R. Cao, Y. Gong, J. Wang, N. Liu, Z. Chen, L. Wang, M. Ishikawa, Z. Gong, *Advanced Materials Technologies* **2020**, 5, 2000549.
[29] L. Xu, Z. Huang, Z. Deng, Z. Du, T. L. Sun, Z.-H. Guo, K. Yue, *Advanced Materials* **2021**, 33, 2105306.
[30] S. Xiang, F. Zheng, S. Chen, Q. Lu, *ACS Applied Materials & Interfaces* **2021**, 13, 20653.
[31] Z.-H. Wang, B.-W. Liu, F.-R. Zeng, X.-C. Lin, J.-Y. Zhang, X.-L. Wang, Y.-Z. Wang, H.-B. Zhao, *Science Advances* 8, eadd8527.

[32] Y. Zhou, M. Chen, Q. Ban, Z. Zhang, S. Shuang, K. Koynov, H.-J. Butt, J. Kong, S. Wu, *ACS Macro Letters* **2019**, 8, 968.
[33] S. Ito, H. Akiyama, R. Sekizawa, M. Mori, M. Yoshida, H. Kihara, *ACS Applied Materials & Interfaces* **2018**, 10, 32649.
[34] L. Kortekaas, J. Simke, D. W. Kurka, B. J. Ravoo, *ACS Applied Materials & Interfaces* **2020**, 12, 32054.
[35] Q. Wang, V. Diez-Cabanes, S. Dell'Elce, A. Liscio, B. Kobin, H. Li, J.-L. Brédas, S. Hecht, V. Palermo, E. J. W. List-Kratochvil, J. Cornil, N. Koch, G. Ligorio, *ACS Applied Nano Materials* **2019**, 2, 1102.
[36] Y. Gu, E. A. Alt, H. Wang, X. Li, A. P. Willard, J. A. Johnson, *Nature* **2018**, 560, 65.
[37] A. M. Asadirad, S. Boutault, Z. Erno, N. R. Branda, *Journal of the American Chemical Society* **2014**, 136, 3024.
[38] K. Imato, K. Momota, N. Kaneda, I. Imae, Y. Ooyama, *Chemistry of Materials* **2022**, 34, 8289.
[39] T. J. Gately, W. Li, S. H. Mostafavi, C. J. Bardeen, *Macromolecules* **2021**, 54, 9319.
[40] L. Yu, Y. Hou, W. Xie, J. L. Cuellar-Camacho, Q. Wei, R. Haag, *Advanced Materials* **2020**, 32, 2006986.
[41] M. Aizawa, H. Akiyama, Y. Matsuzawa, *Advanced Engineering Materials* **2022**, 24, 2100823.
[42] Y. Zhou, C. Zhang, S. Gao, W. Li, J.-j. Kai, Z. Wang, *ACS Applied Materials & Interfaces* **2021**, 13, 50451.
[43] Z. Wang, L. Guo, H. Xiao, H. Cong, S. Wang, *Materials Horizons* **2020**, 7, 282.
[44] S. Wang, W. H. Hu, Y. Nakamura, N. Fujisawa, A. E. Herlyng, M. Ebara, M. Naito, *Advanced Functional Materials* **2023**, 33, 2215064.
[45] M. Inada, T. Horii, T. Fujie, T. Nakanishi, T. Asahi, K. Saito, *Materials Advances* **2023**, 4, 1289.
[46] P. D. McFadden, K. Frederick, L. A. Argüello, Y. Zhang, P. Vandiver, N. Odegaard, D. A. Loy, *ACS Applied Materials & Interfaces* **2017**, 9, 10061.
[47] V. X. Truong, K. Ehrmann, M. Seifermann, P. A. Levkin, C. Barner-Kowollik, *Chemistry – A European Journal* **2022**, 28, e202104466.
[48] V. X. Truong, *ChemPhotoChem* **2020**, 4, 564.
[49] A. C. Fonseca, M. S. Lima, A. F. Sousa, A. J. Silvestre, J. F. J. Coelho, A. C. Serra, *Polymer Chemistry* **2019**, 10, 1696.
[50] W. L. Koay, C. Gao, Q. T. Vu, X. Y. Oh, H. Lin, S. Mondal, N. D. P. Singh, X. J. Loh, M. T. N. Le, V. X. Truong, *Biomacromolecules* **2024**, 25, 6635.
[51] I. M. Irshadeen, S. L. Walden, M. Wegener, V. X. Truong, H. Frisch, J. P. Blinco, C. Barner-Kowollik, *Journal of the American Chemical Society* **2021**, 143, 21113.
[52] K. Kalayci, H. Frisch, C. Barner-Kowollik, V. X. Truong, *Advanced Functional Materials* **2020**, 30, 1908171.
[53] V. X. Truong, F. Li, F. Ercole, J. S. Forsythe, *ACS Macro Letters* **2018**, 7, 464.
[54] A. Ahmadalinezhad, A. Sayari, *Physical Chemistry Chemical Physics* **2014**, 16, 1529.
[55] C. Yan, A. Sayari, *Chemical Engineering Journal* **2024**, 479, 147498.
[56] S. D. Tobing, A. Klein, *Journal of Applied Polymer Science* **2001**, 79, 2230.
[57] S. Tobing, A. Klein, L. H. Sperling, B. Petrasko, *Journal of Applied Polymer Science* **2001**, 81, 2109.
[58] S. Sun, M. Li, A. Liu, *International Journal of Adhesion and Adhesives* **2013**, 41, 98.

Reported herein is a versatile adhesive platform based on a redshifted [2+] photocycloaddition mechanism. The visible light-cured adhesive is robust, moisture-tolerant and thermally stable, yet can be readily debonded under long-wavelength UV light irradiation.

Xin Yi Oh, Quyen Thi Vu, Michelle Yu Mei Ling, Mohammad Izadyar, Syed Ali Abbas Abedi, Xiaogang Liu, Vinh X. Truong**

Moisture Tolerance, Thermally Stable and Light Switchable Adhesives Platform Based on Reversible Redshifted [2+2] Photocycloaddition

ToC figure

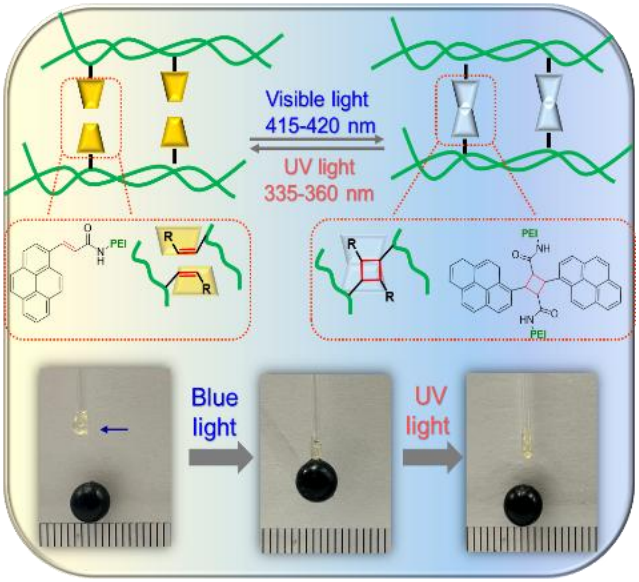

Supporting Information

Moisture Tolerance, Thermally Stable and Light Switchable Adhesives Platform Based on Reversible Redshifted [2+2] Photocycloaddition

Xin Yi Oh, Quyen Thi Vu, Michelle Yu Mei Ling, Syed Ali Abbas Abedi, Mohammad Izadyar, Xiaogang Liu, Vinh X. Truong**

1. Characterization Methods

^{1}H NMR spectra were recorded on a Bruker spectrometer (400 MHz) at ambient temperature. DMSO-d_6 and D_2O (Cambridge Isotope Laboratories, USA) were used as the solvents for the NMR analysis, and the chemical shift was calibrated using residual undeuterated solvents or tetramethylsilane (TMS) as the internal standard.

UV-Vis Spectra were recorded on a PerkinElmer LAMBDA Series UV/Vis/NIR 950 spectrophotometer equipped with a photomultiplier detector. Samples were prepared in water or DMSO and measured in Hellma Analytics quartz high precision cells with a path length of 10 mm at ambient temperature.

Light irradiation on small molecule and polymer solutions was performed using commercial LED light with wavelengths at λ_{max} = 335–355 nm or 420 nm, respectively. LED emission spectra were recorded using an Ocean Insight Flame-T-UV-Vis spectrometer, with an active range of 200–850 nm and an integration time of 10 ms.

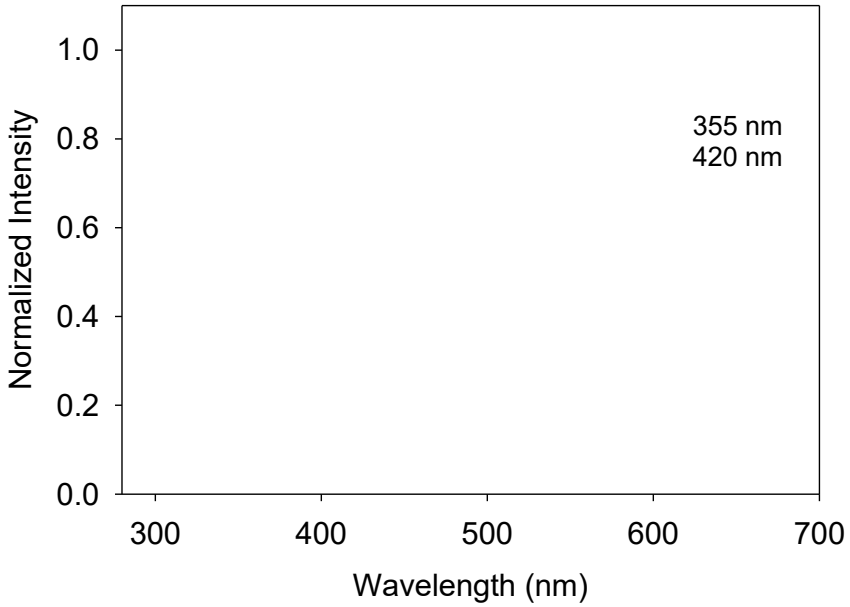

Figure S1. Emission spectra of the LED sources centered at 355 nm and 420 nm.

Rheological experiments were conducted using an Anton Paar Physical rheometer with a plate-plate configuration. The lower plate is made of quartz and the upper plate is made of stainless steel with a diameter of 25 mm. A liquid light guild, which was connected to an OmniCure S2000 white light with a filter cut off at λ = 400–500 nm, was placed directly underneath the quartz plate, and the light intensity was adjusted at I = 20 mW cm^{-2}. In a typical measurement, the polymer solution (100 μL) was placed on the quartz plate and the upper plate was brought down to a gap of 0.2 mm. The test was started by applying a 1% strain with a frequency of 0.1 Hz on the sample. After a period of 1 min, the LED light was switched on to initiate the photopolymerization.

To investigate the stability of photocrosslinked **AP$_1$-PEI** under heating environment, the light was turned off for 10 min. Then, the temperature was increased and stabilized at 70 °C.

High resolution mass spectra (HRMS) were recorded on an Agilent 6210 Series 1969A ESI-TOF (time of flight) mass spectrometer using EI (electron ionization) or ESI (electrospray

ionization). Liquid chromatography–mass spectrometry (LCMS) was recorded on an Agilent Single Quadrupole using atmospheric pressure ionization (API).

Fourier transform infrared spectra (FTIR) were recorded on Bruker, FTIR, HYPERION 3000 by accumulating of 32 scans at 4 cm^{-1} of resolution.

Scanning Electron Microscopy (SEM) Measurements. The morphology of as-prepared adhesive layers was observed by scanning electron microscopy (SEM, JEOL/Oxford, JSM7900FLV/X-Max80), operated at 5 kV. The sample was coated with gold for 120 s at 20 mA before the measurements.

Lap shear test was measured on a universal testing machine (Instron model 5569), equipped with a 1 kN load cell at a speed of 1 mm/min, in accordance with standard test method ASTM D1002, using pneumatic side action tensile grips. Adhesive strength of the specimens was recorded by the Bluehill 3 software. Samples were prepared according to the following diagram. Triplicate samples for each adhesive test were prepared and the mean adhesive strengths were calculated.

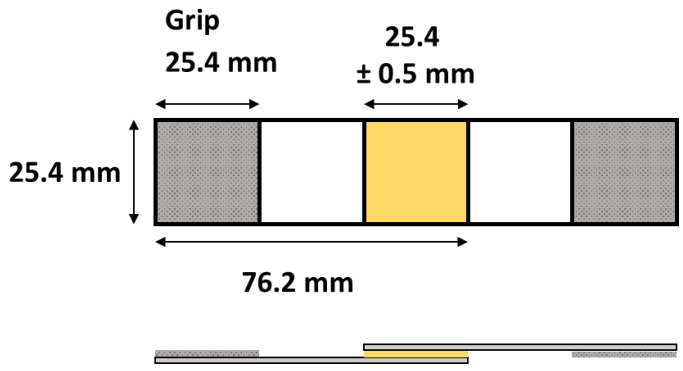

2. Computational Methods and Additional Computational Results

This work used Gaussian 16A to conduct Density Functional Theory (DFT) and Time-Dependent DFT (TD-DFT) calculations.[1] Unless stated otherwise, all structure optimizations were performed without constraints using the M06-2X functional combined with the def2-SVP basis set.[2,3] We applied GD3 correction in all calculations.[4] Solvation effects in DMSO were considered using the SMD model.[5] The excitation and de-excitation energies of all molecules were calculated using state-specific equilibrium solvation (corrected linear solvation or cLR formalism) at the TD-DFT-M062X/def2SVP level of theory in DMSO.[6]

The ethyl group of **1** was replaced with a methyl group to reduce the computational load.

Frequency calculations confirmed that we obtained stable structures without imaginary vibration frequencies in both the ground and excited states. The M06-2X functional was chosen because it is suitable for structural optimizations of organic molecules and calculations of electronic excitation energies.

The energy of the Franck-Condon state and the locally excited states of the monomer-monomer complex was calculated by summing the electronic energy of one monomer in the excited state and the other monomer in the ground state, treating both monomers separately. The energy of the monomer-monomer complex in the ground state was calculated by multiplying the energy of a monomer by two.

The geometry of the monomer-monomer complex was placed arbitrarily, as we assumed they are far away from each other and have no interactions, unlike in the dimeric form.

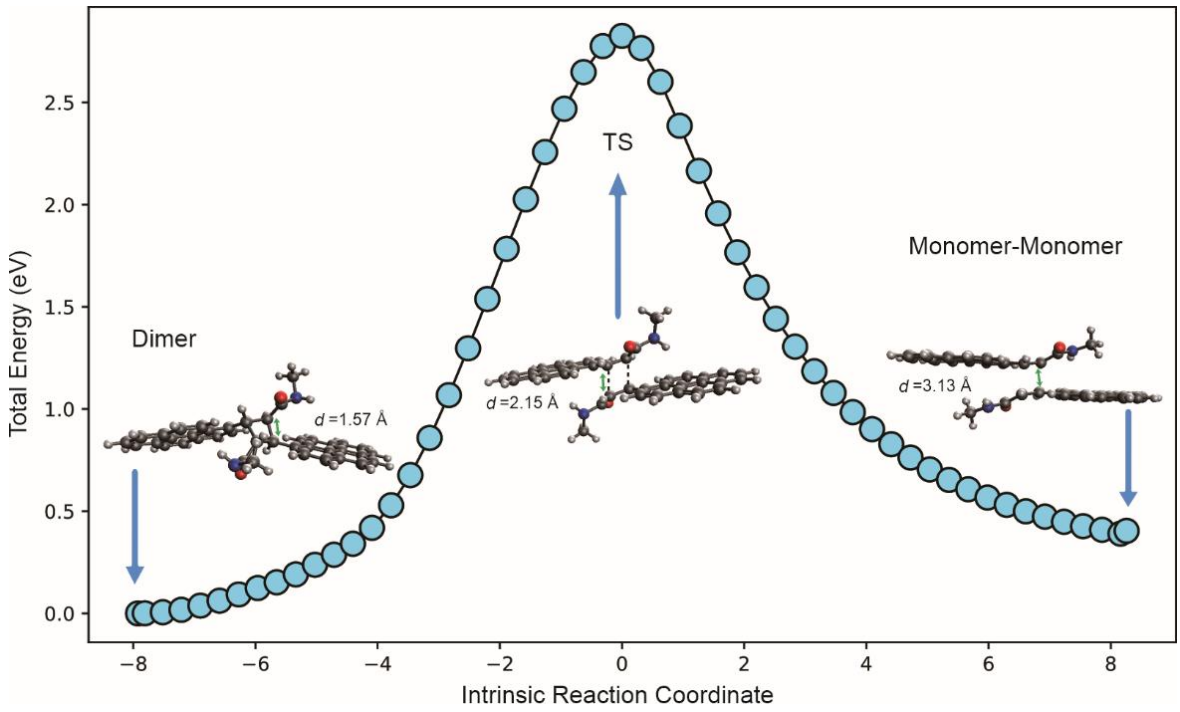

Figure S2. A reaction pathway's energy profile illustrates the transition from a monomer-monomer to a dimer state. The graph plots total energy (electron volts, eV) against the intrinsic reaction coordinate. Critical points on the curve include the dimer state at the far left with a bond distance (*d*) of 1.57 Å, the transition state (TS) at the peak with a distance of 2.15 Å, and the monomer-monomer state at the far right with a distance of 3.13 Å.

This figure illustrates the energy profile associated with the transformation between the monomer-monomer and dimer forms of a molecular system. The dimer state is depicted at an energy minimum with a bond distance (d) of 1.57 Å. Proceeding rightward along the x-axis, the system encounters a transition state (TS), marked at an energy peak of 2.67 eV and a bond distance of 2.15 Å. Beyond the TS, the curve descends towards the monomer-monomer state, shown at the far right, where the molecule is in its less stable form. In this form, the bond distance *d* increases to 3.13 Å, suggesting the separation of the two moieties to form two independent monomers.

After absorption, the dimer first reaches the Franck-Condon state (D*(FC)) at an energy of 3.94 eV. From there, it transitions to the locally excited state (D*(LE)) at 3.73 eV. Subsequently, the molecule proceeds to the charge transfer state (D*(CT)) at 3.19 eV, followed by deexcitation to the ground state. Due to this stable, non-emissive CT state ($f = 0$), the dimer is less fluorescent than the monomer.

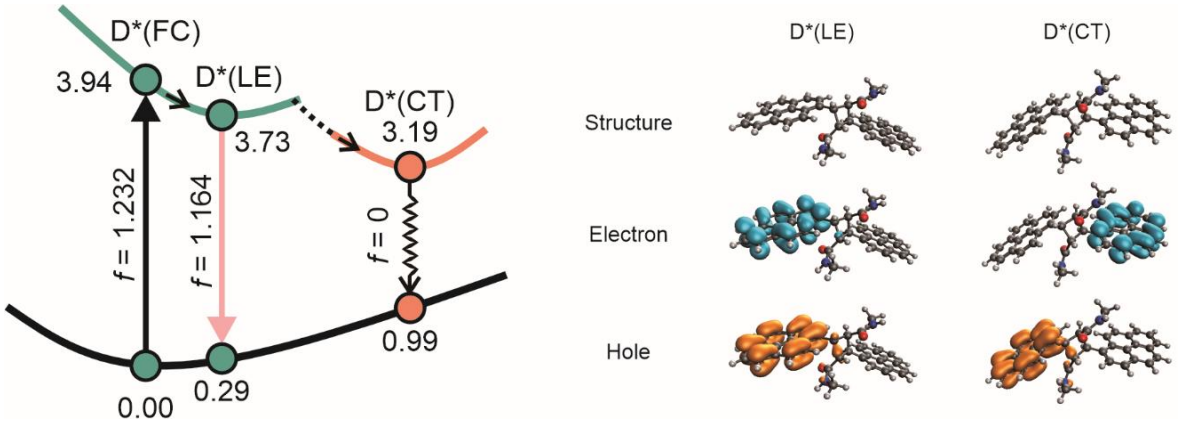

Figure S3. (a) Energy levels with Franck-Condon state (D*(FC)), locally excited state (D*(LE)), and charge transfer state (D*(CT)). For clarity, the corresponding energies in electron volts (eV) are not drawn in scale. (b) Molecular structures in the D*(LE) and D*(CT) states and electron and hole distributions. The structures depict changes in electron density (shown in blue) and hole density (shown in orange), which helps visualize the charge transfer within the molecule upon excitation.

3. Additional Data

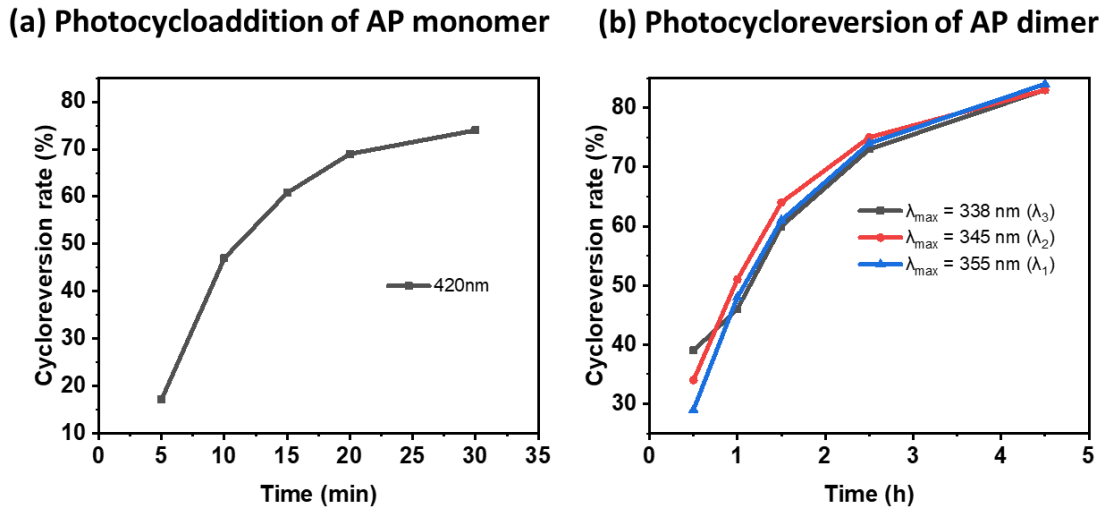

Figure S4. Kinetics of (a) photocycloaddition of AP monomer at λ_{max} = 420 nm (intensity I = 20 mW·cm^{-2}). (b) photocycloreversion of AP dimer at different wavelength range from 335–360 nm at the intensity I = 4.14–4.78 mW·cm^{-2}.

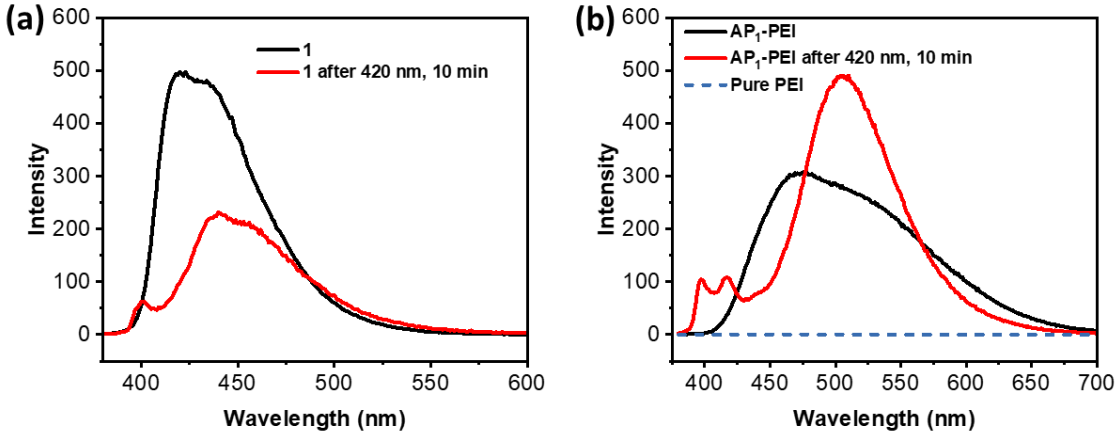

Figure S5. Fluorescence spectra of **(a)** compound **1** before and after irradiated with blue light, and (**b**) **AP$_1$-PEI** before and after blue light irradiation, PEI does not show any fluorescent emission.

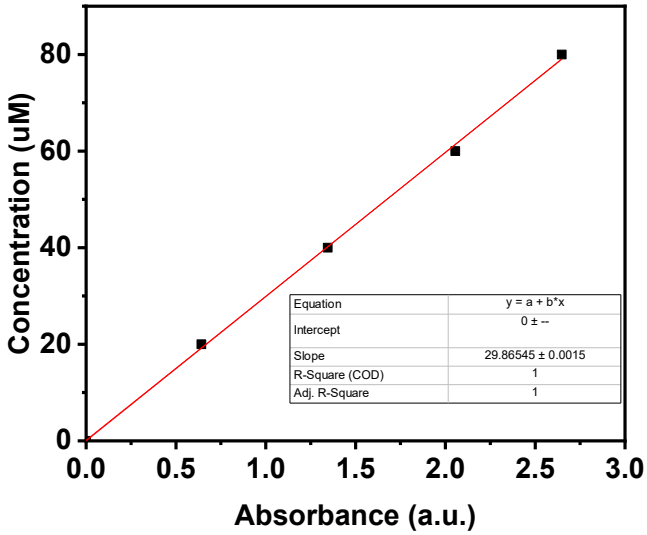

Figure S6. Calibration curve to study the degree of substitution of **AP** in PEI (from UV-Vis absorbance of the small molecule **AP).**

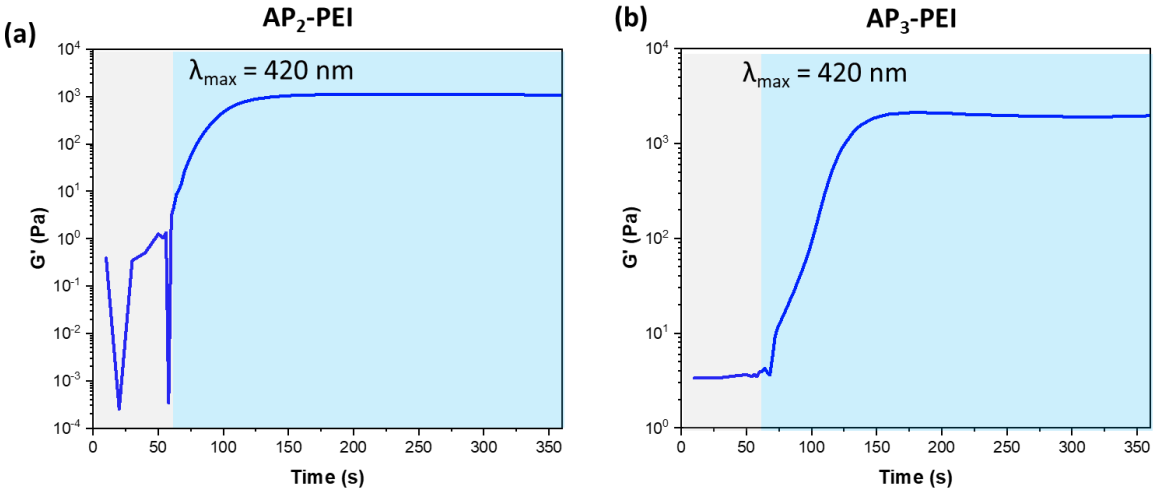

Figure S7. Rheological assessment (time sweep) of (a)**AP$_2$-PEI** and (b)**AP$_3$-PEI** in 30 wt% in water under irradiation of blue light (λ_{max} = 420 nm, I = 20 mW·cm^{-2}), showing the rapid increase of G' value but not to a higher extent even with higher proportion of AP units.

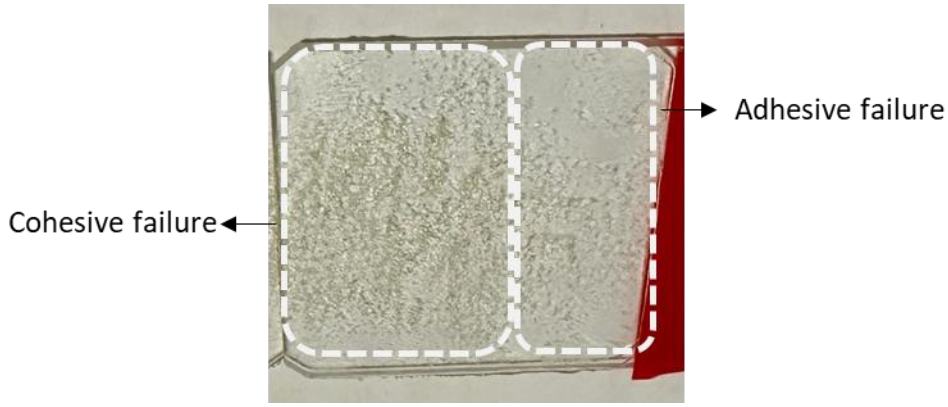

Figure S8. Glass substrate after UV irradiation (λ_{max} = 340 nm, I = 10 mW cm^{-2}), showing cohesive and adhesive failure.

4. Synthetic procedure

4.1 Materials

1-Pyrenecarboxaldehyde (>98.0%, Tokyo Chemical Industry (TCI), Japan), malonic acid (>99.0%, TCI), pyridine (>99.0%, TCI), piperidine (≥99%, Sigma-Aldrich, USA), hydrochloric acid (37%, Sigma-Aldrich), anhydrous tetrahydrofuran (≥99.9%, Sigma-Aldrich), 1-(3-dimethylaminopropyl)-3-ethylcarbodiimide hydrochloride (>98.0%, TCI), *N*-hydroxy succinimide (>98.0%, TCI), anhydrous *N,N*-dimethylformamide (≥99.8%, Sigma-Aldrich), propylamine (>98.0%, TCI), polyethylene imine (PEI) (average M_w ~25,000 by LS, average M_n ~10,000 by GPC, branched) (Sigma-Aldrich).

4.2 Synthesis of 3-(1-pyrenyl)acrylic acid

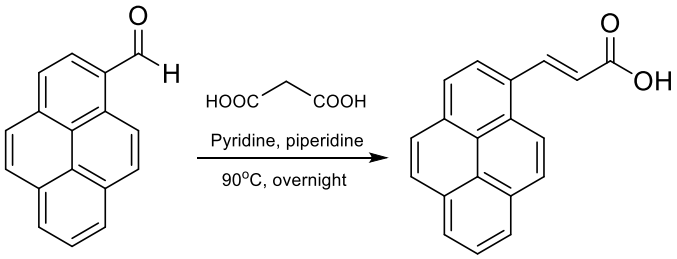

To a 250 mL-round bottom flask equipped with a stirrer bar were added 1-pyrenecarboxaldehyde (5 g, 21.7 mmol), malonic acid (4.16 g, 40.0 mmol), pyridine (26 mL),

and piperidine (8 mL). The mixture was heated for 16 h at 90 °C and cooled to room temperature before slowly transferred to a beaker containing ice water. The mixture was added to iced cooled hydrochloric acid solution (1M, 200 mL). The precipitate was filtered and collected as a yellow powder (5.03 g, 85%).

^{1}H NMR (400 MHz, DMSO-d_6) δ 8.69 (d, J = 12 Hz, 1H), 8.51 (t, J = 8 Hz, 2H), 8.36 – 8.09 (m, 8H), 6.83 (d, J = 12 Hz, 1H) ppm;

^{13}C NMR (101 MHz, DMSO-d_6) δ 167.7, 139.8, 132.0, 130.8, 130.1, 128.9, 128.6, 128.4, 127.8, 127.3, 126.5, 126.1, 125.8, 125.3, 124.5, 124.0, 123.8, 122.2, 121.7 ppm;

HRMS m/z: $[M + H]^+$ calcd for $C_{19}H_{12}O_2$, 273.0904 found 273.0904.

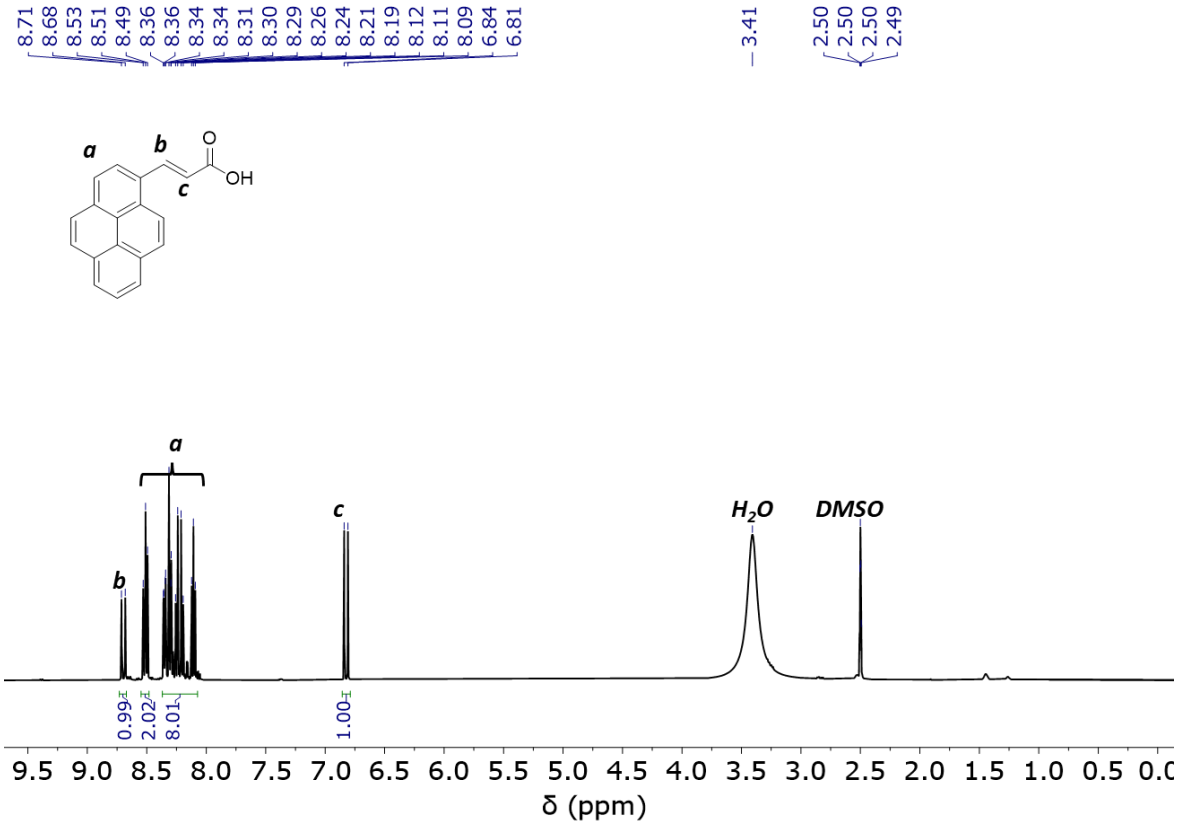

Figure S9. ^{1}H NMR spectrum of 3-(1-pyrenyl)acrylic acid (400 MHz, 298 K, DMSO-d_6).

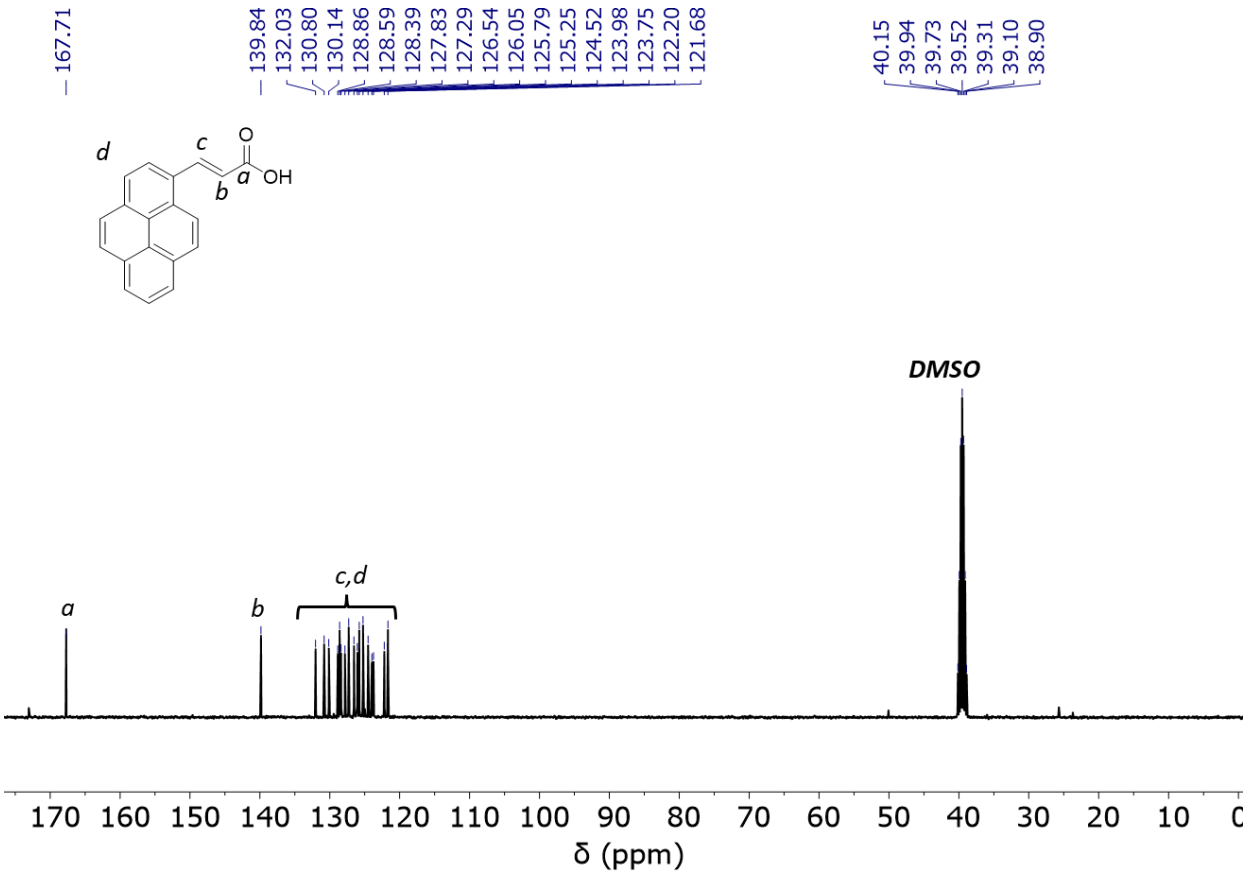

Figure S10. ^{13}C NMR spectrum of 3-(1-pyrenyl)acrylic acid (101 MHz, 298 K, DMSO-d_6).

4.3 Synthesis of acryl pyrene with *N*-hydroxy succinimide ester

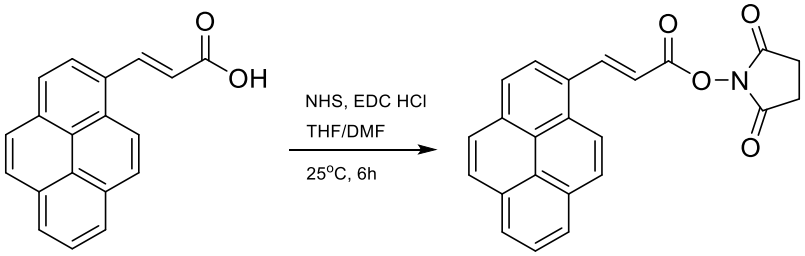

To a 250 mL-round bottom flask equipped with a stirrer bar were added 3-(1-pyrenyl)acrylic acid (1 g, 3.67 mmol), EDC HCl (0.84 g, 4.40 mmol), *N*-hydroxy succinimide (0.51 g, 4.40 mmol), anhydrous THF (20 mL), and anhydrous DMF (5 mL). The mixture was stirred for 6 h at room temperature before slowly transferred to a beaker containing ice water. The mixture was added to iced cooled distilled water (100 mL). The precipitate was filtered then dried in vacuum at 40 °C and collected as a yellow powder (1.14 g, 84%).

^{1}H NMR (400 MHz, DMSO-d_6) δ 9.05 (d, J = 16.0 Hz, 1H), 8.72 (d, J = 8.0 Hz, 1H), 8.64 (d, J = 12 Hz, 1H), 8.43 – 8.13 (m, 7H), 7.30 (d, J = 16.0 Hz, 1H), 2.91 (s, 4H) ppm;

^{13}C NMR (101 MHz, DMSO-d_6) δ 170.5, 162.4, 145.4, 133.1, 130.7, 130.0, 129.6, 129.2, 129.1, 127.3, 126.7, 126.5, 126.4, 126.3, 125.2, 125.0, 123.8, 123.5, 122.0, 113.2, 54.9, 25.6 ppm;

HRMS m/z: $[M + Na]^+$ calcd for $C_{23}H_{15}NO_4$, 392.0882 found 392.0882.

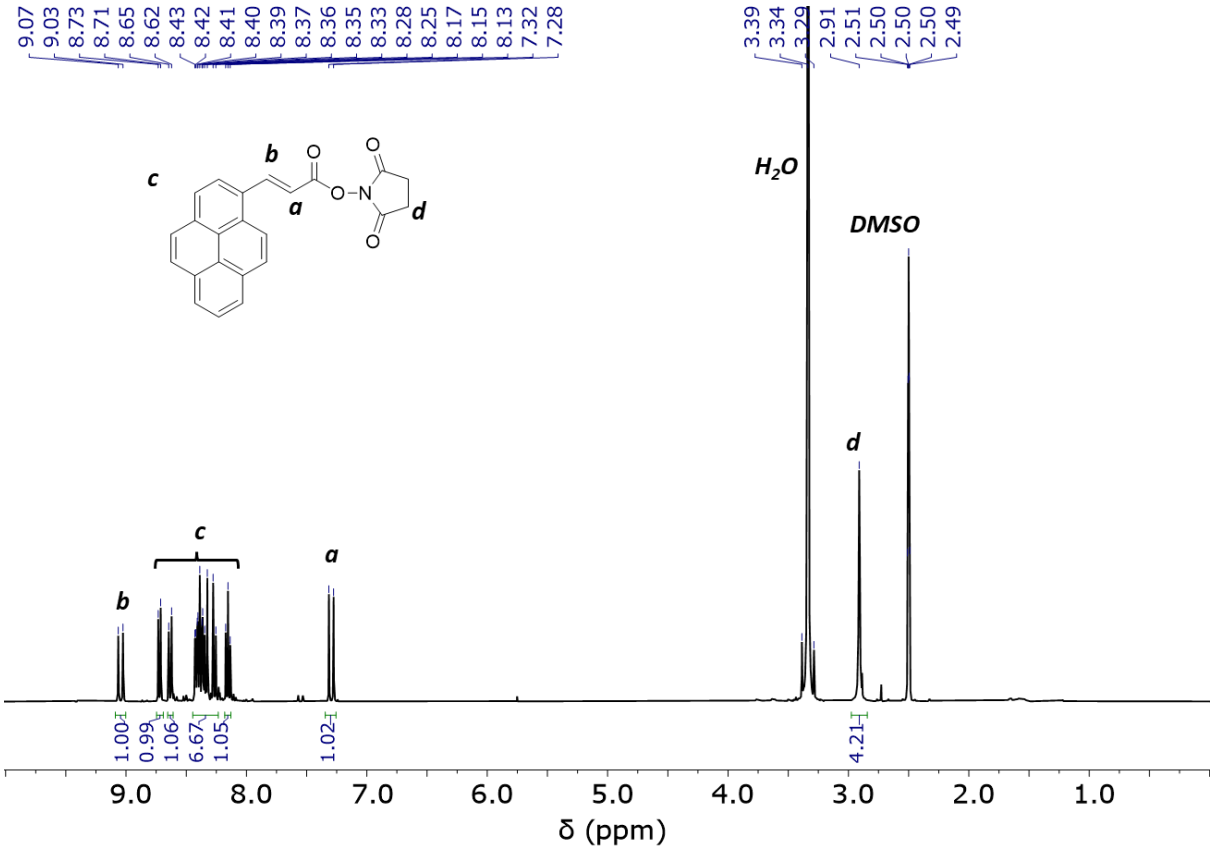

Figure S11. ^{1}H NMR spectrum of acryl pyrene with *N*-hydroxy succinimide ester (400 MHz, 298 K, DMSO-d_6).

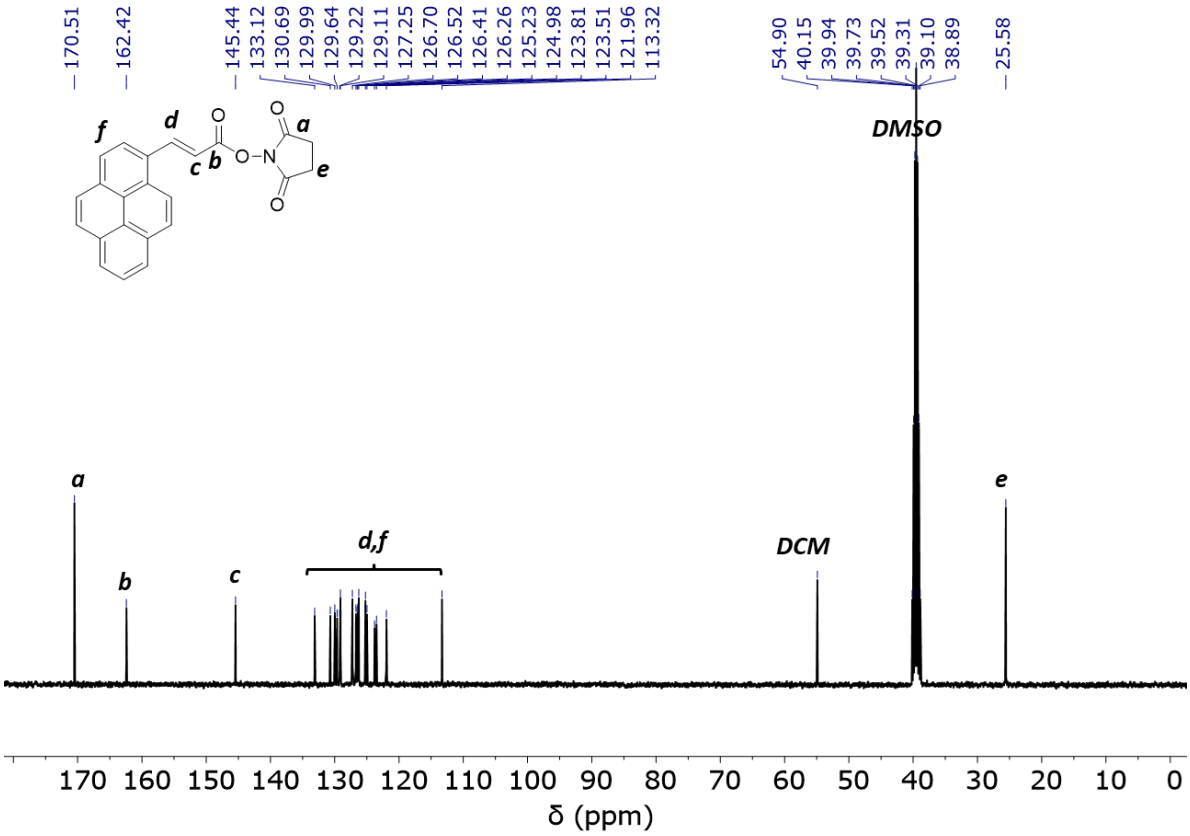

Figure S12. ^{13}C NMR spectrum of acryl pyrene with *N*-hydroxy succinimide ester (101 MHz, 298 K, DMSO-d_6).

4.4 Synthesis of acryl pyrene amide (1)

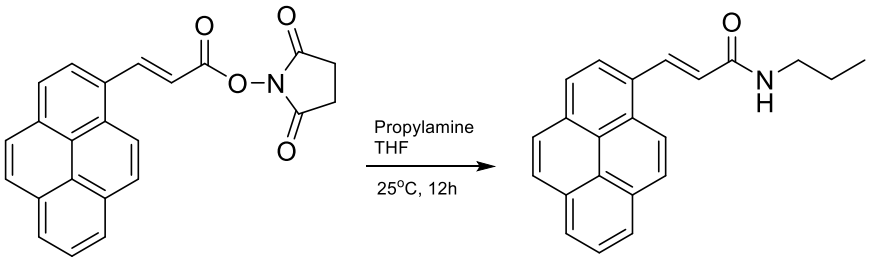

1

To a 250 mL-round bottom flask equipped with a stirrer bar were added acryl pyrene with *N*-hydroxy succinimide ester (0.2 g, 0.54 mmol), propylamine (0.84 g, 4.40 mmol), and anhydrous THF (5 mL). The mixture was stirred for 6 h at room temperature before slowly transferred to a beaker containing ice water. The mixture was added to iced cooled distilled

water (100 mL). The precipitate was filtered then dried in vacuum at 40 °C and collected as a yellow powder (1.14 g, 84%).

^{1}H NMR (400 MHz, DMSO-d_6) δ 8.53 – 8.49 (m, 2H), 8.36 – 8.09 (m, 10H), 6.92 (d, J = 16 Hz, 1H), 3.23 (q, J = 4 Hz, 2H), 1.52 (sx, J = 8 Hz, 2H), 0.93 (t, J = 8 Hz, 3H) ppm;

^{13}C NMR (101 MHz, DMSO-d_6) δ 164.9, 134.6, 131.5, 130.9, 130.3, 129.0, 128.6, 128.4, 128.1, 127.4, 126.6, 125.9, 125.6, 125.4, 124.1, 123.9, 122.6, 40.6, 22.5, 11.5 ppm;

LC-MS (ES-API, *m/z*) [MH$^+$] 314.2 (100%).

HRMS *m/z*: [M + H]$^+$ calcd for $C_{22}H_{19}NO$, 314.1527 found 314.1527.

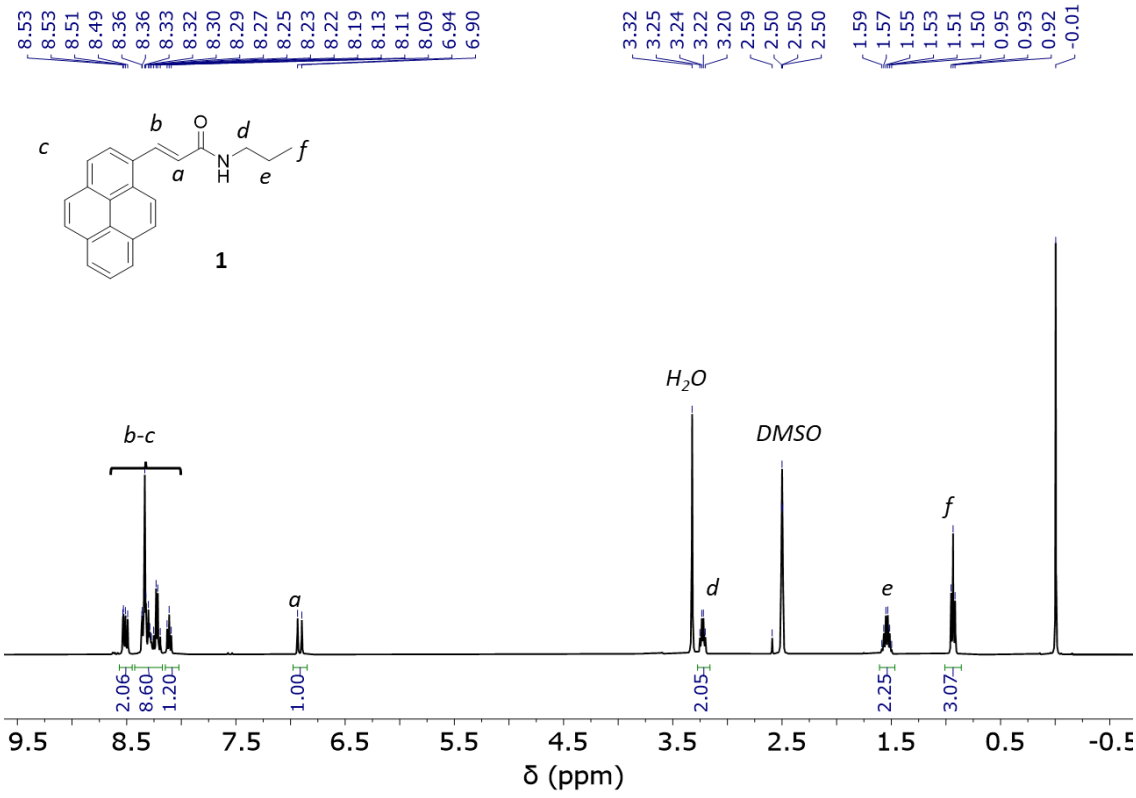

Figure S13. ^{1}H NMR spectrum of acryl pyrene amide (1) (400 MHz, 298 K, DMSO-d_6).

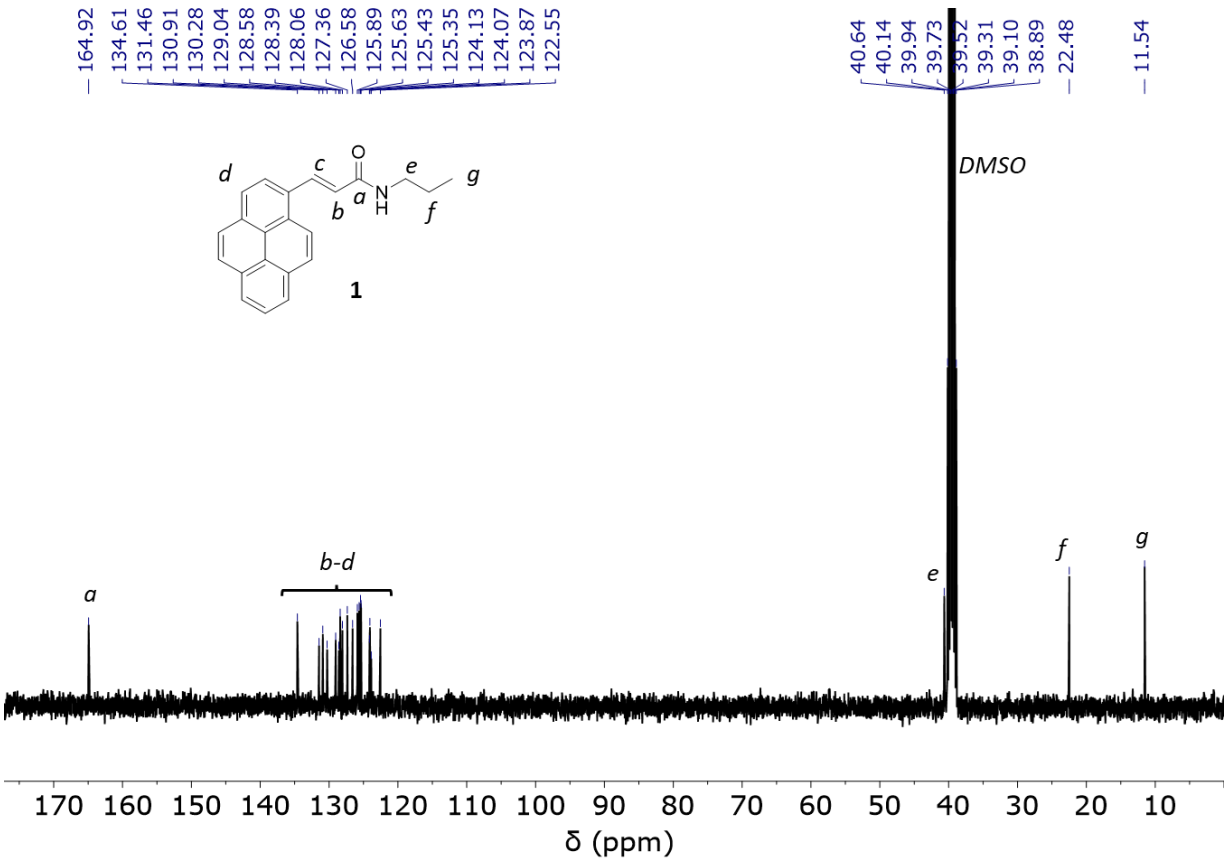

Figure S14. ^{13}C NMR spectrum of acryl pyrene amide (1) (101 MHz, 298 K, DMSO-d_6).

4.5 Synthesis of AP-PEI

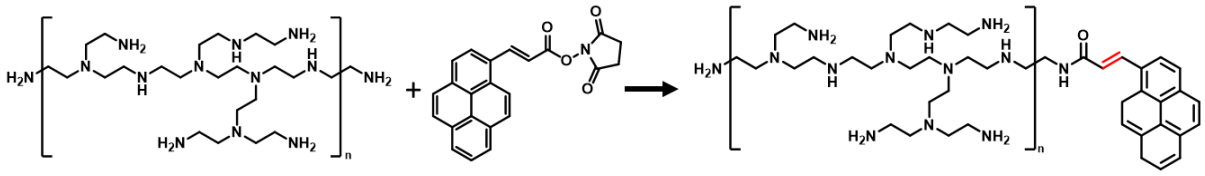

In a typical formulation, acryl pyrene-containing polyethyleneimine (**AP-PEI**) was prepared by mixing polyethylene imine (PEI) (M_n = 10 000 g/mol) and acryl pyrene with *N*-hydroxy succinimide ester in *N,N*-dimethylformamide (20 mL) at room temperature. After 12 h, the mixture was dialyzed against water for 3 days and removed any precipitate via centrifugation, then freeze-dried to obtain yellow liquid of **AP-PEI**. **AP-PEI** with different ratios of AP and PEI were prepared according to **Table S1**.

^{1}H NMR (400 MHz, D_2O) δ 8.08 (s), 3.47 – 2.67 (m) ppm

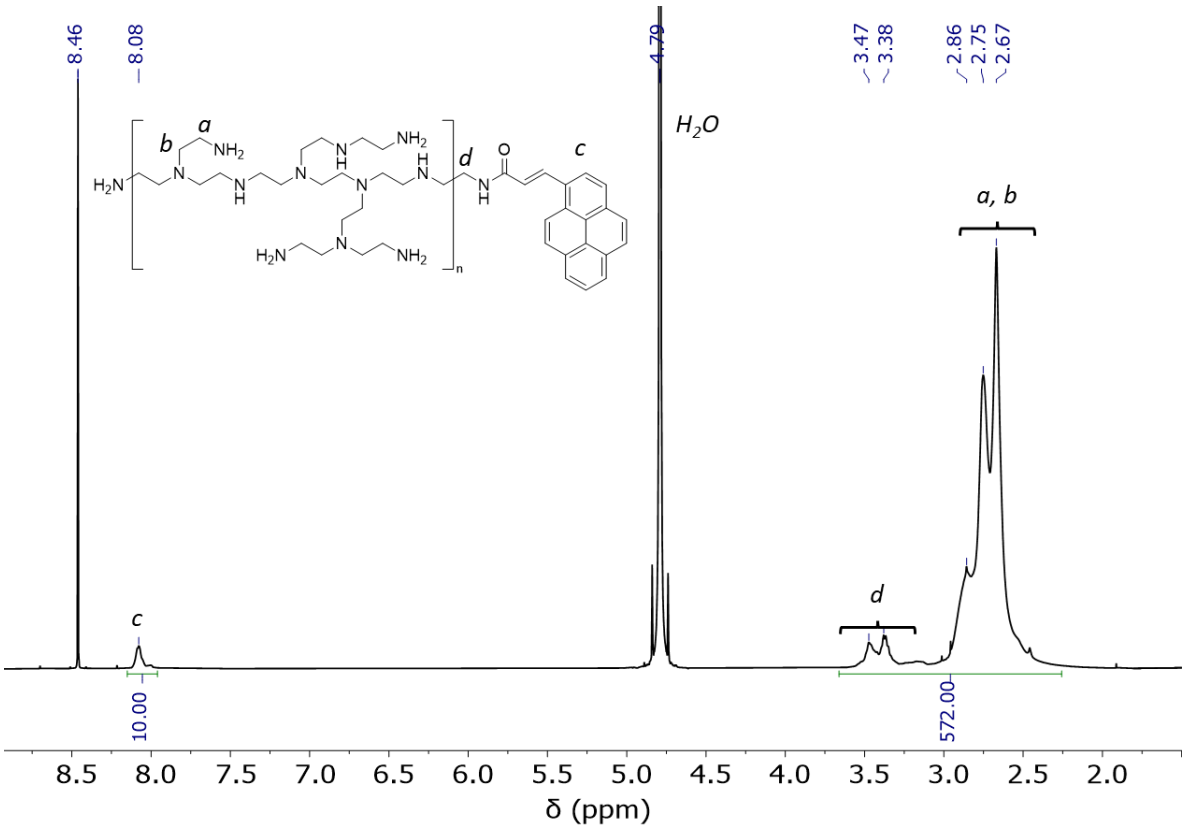

Figure S15. ^{1}H NMR spectrum of **AP$_1$-PEI** (400 MHz, 298 K, D_2O).

Table S1. Synthesis of **AP-PEI** with different ratios of AP and PEI.

Entry	**PEI**	**AP**	**AP-PEI (molar ratio)**
AP$_1$-PEI	2 g	73.9 mg	1:1
AP$_2$-PEI	2 g	147.6 mg	2:1
AP$_3$-PEI	2 g	221.6 mg	3:1

Table S2. Adhesive systems based on chromophores that can participate in reversible photocycloaddition systems.

Entries	Polymer matrix	Maximum adhesion (substrate, method)	Activation / deactivation stimuli	References
[4+4] photodimerization of anthracenes				
1	Di9AC-Si_amide	10N/10mm (peel strength, with molecular layer)	405 nm / 254 nm	41
2	p(BA-AA)-*g*-An with p(DMA-BA)	~10.1 kPa (glass, pull-off adhesion test)	405 nm / -	42
3	9-anth-PEI glue PEI-60K	606.7 ± 30.3 kPa (quartz, tensile strength)	>400 nm / 70°C	43
[2+2] photodimerization of cinnamate				
4	poly((E)-2-((3-(3,4-dihydroxyphenyl)acryloyl)oxy)ethyl acrylate-co-2-ethylhexylmethacrylate) (Poly1f)	6 MPa (aluminum, tensile strength)	365 nm & 120°C / 254 nm	44
[2+2] photodimerization of coumarin				
5	2,4,6,8-tetramethyl-2,4,6,8-tetrakis(propylglycidylether)cyclotetrasiloxane with 7-hydoxycoumarin (SS1)	~1.7 MPa (glass, tensile strength)	365 nm / 254 nm	45

References

(1) Frisch, M. J.; Trucks, G. W.; Schlegel, H. B.; Scuseria, G. E.; Robb, M. A.; Cheeseman, J. R.; Scalmani, G.; Barone, V.; Petersson, G. A.; Nakatsuji, H.; Li, X.; Caricato, M.; Marenich, A. V.; Bloino, J.; Janesko, B. G.; Gomperts, R.; Mennucci, B.; Hratchian, H. P.; Ortiz, J. V.; Izmaylov, A. F.; Sonnenberg, J. L.; Williams; Ding, F.; Lipparini, F.; Egidi, F.; Goings, J.; Peng, B.; Petrone, A.; Henderson, T.; Ranasinghe, D.; Zakrzewski, V. G.; Gao, J.; Rega, N.; Zheng, G.; Liang, W.; Hada, M.; Ehara, M.; Toyota, K.; Fukuda, R.; Hasegawa, J.; Ishida, M.; Nakajima, T.; Honda, Y.; Kitao, O.; Nakai, H.; Vreven, T.; Throssell, K.; Montgomery Jr., J. A.; Peralta, J. E.; Ogliaro, F.; Bearpark, M. J.; Heyd, J. J.; Brothers, E. N.; Kudin, K. N.; Staroverov, V. N.; Keith, T. A.; Kobayashi, R.; Normand, J.; Raghavachari, K.;

Rendell, A. P.; Burant, J. C.; Iyengar, S. S.; Tomasi, J.; Cossi, M.; Millam, J. M.; Klene, M.; Adamo, C.; Cammi, R.; Ochterski, J. W.; Martin, R. L.; Morokuma, K.; Farkas, O.; Foresman, J. B.; Fox, D. J.: Gaussian 16 Rev. C.01. Wallingford, CT, 2016.

(2) Walker, M.; Harvey, A. J.; Sen, A.; Dessent, C. E. Performance of M06, M06-2X, and M06-HF density functionals for conformationally flexible anionic clusters: M06 functionals perform better than B3LYP for a model system with dispersion and ionic hydrogen-bonding interactions. The Journal of Physical Chemistry A 2013, 117, 12590-12600.

(3) Weigend, F.; Ahlrichs, R. Balanced basis sets of split valence, triple zeta valence and quadruple zeta valence quality for H to Rn: Design and assessment of accuracy. Physical Chemistry Chemical Physics 2005, 7, 3297-3305.

(4) Grimme, S.; Antony, J.; Ehrlich, S.; Krieg, H. A consistent and accurate ab initio parametrization of density functional dispersion correction (DFT-D) for the 94 elements H-Pu. The Journal of Chemical Physics 2010, 132.

(5) Tomasi, J.; Mennucci, B.; Cammi, R. Quantum Mechanical Continuum Solvation Models. Chemical Reviews 2005, 105, 2999-3094.

(6) Caricato, M. A corrected-linear response formalism for the calculation of electronic excitation energies of solvated molecules with the CCSD-PCM method. Computational and Theoretical Chemistry 2014, 1040-1041, 99-105.